J. Fluid Mech. (2019), *vol.* 862, *pp.* 162–199. © Cambridge University Press 2019
doi:10.1017/jfm.2018.954

A simple system for moist convection: the Rainy–Bénard model

Geoffrey K. Vallis[1,†], **Douglas J. Parker**[2] **and Steven M. Tobias**[3]

[1]Department of Mathematics, University of Exeter, Exeter EX4 4QF, UK

[2]School of Earth and Environment, University of Leeds, Leeds LS2 9JT, UK

[3]Department of Applied Mathematics, University of Leeds, Leeds LS2 9JT, UK

(Received 17 March 2018; revised 18 October 2018; accepted 17 November 2018; first published online 9 January 2019)

Rayleigh–Bénard convection is one of the most well-studied models in fluid mechanics. Atmospheric convection, one of the most important components of the climate system, is by comparison complicated and poorly understood. A key attribute of atmospheric convection is the buoyancy source provided by the condensation of water vapour, but the presence of radiation, compressibility, liquid water and ice further complicate the system and our understanding of it. In this paper we present an idealized model of moist convection by taking the Boussinesq limit of the ideal-gas equations and adding a condensate that obeys a simplified Clausius–Clapeyron relation. The system allows moist convection to be explored at a fundamental level and reduces to the classical Rayleigh–Bénard model if the latent heat of condensation is taken to be zero. The model has an exact, Rayleigh-number-independent 'drizzle' solution in which the diffusion of water vapour from a saturated lower surface is balanced by condensation, with the temperature field (and so the saturation value of the moisture) determined self-consistently by the heat released in the condensation. This state is the moist analogue of the conductive solution in the classical problem. We numerically determine the linear stability properties of this solution as a function of Rayleigh number and a non-dimensional latent-heat parameter. We also present some two-dimensional, time-dependent, nonlinear solutions at various values of Rayleigh number and the non-dimensional condensational parameters. At sufficiently low Rayleigh number the system converges to the drizzle solution, and we find no evidence that two-dimensional self-sustained convection can occur when that solution is stable. The flow transitions from steady to turbulent as the Rayleigh number or the effects of condensation are increased, with plumes triggered by gravity waves emanating from other plumes. The interior dries as the level of turbulence increases, because the plumes entrain more dry air and because the saturated boundary layer at the top becomes thinner. The flow develops a broad relative humidity minimum in the domain interior, only weakly dependent on Rayleigh number when that is high.

Key words: atmospheric flows, condensation/evaporation

† Email address for correspondence: g.vallis@exeter.ac.uk

https://doi.org/10.1017/jfm.2018.954 Published online by Cambridge University Press

1. Introduction

Convection is ubiquitous in fluids, certainly in geophysical and astrophysical settings. In Earth's atmosphere convection is responsible for the towering cumulonimbus of the tropics and plays a major role in mid-latitude storm systems (Emanuel 1994; Smith 2013), and in the ocean convection ventilates the deep abyss (e.g. Marshall & Schott 1999). Convection in the Earth's mantle leads to continental drift (Parsons & McKenzie 1978), and deeper in the fluid outer core convective dynamos produce the magnetic field of Earth and other planets (Schubert & Soderlund 2011). In stars convection enables the heat released by fusion to escape the burning core maintaining a quasi-steady state and leads to stellar magnetic field generation (Brun & Browning 2017).

A classic problem is that of Rayleigh–Bénard convection. Here, in the usual configuration, a Boussinesq fluid is confined between two horizontal plates held at different, constant (in both space and time) temperatures, with the fluid having uniform diffusivities and viscosities, and literally hundreds of papers have been written on this or closely connected problems – see Ahlers, Grossmann & Lohse (2009) or Chillà & Schumacher (2012) for reviews. A solution of no motion then exists, with a uniform gradient of temperature between bottom and top, and temperature diffusing from one plate to the other. If the lower plate is at a higher temperature than the upper one, and the Rayleigh number is sufficiently high, then the diffusive state is linearly unstable (Rayleigh 1916; Chandrasekhar 1961; Drazin & Reid 1981) and convection results. Depending on the value of the controlling non-dimensional parameters (the Rayleigh number, the Prandtl number and the aspect ratio) the ensuing motion may be steady or turbulent, or somewhere in between, with the level of turbulence normally increasing as the Rayleigh number increases. The convecting flow may also coalesce and/or aggregate into various patterns, many of which have been extensively studied numerically and experimentally.

Various theories have also been proposed for how the heat transport scales with the Rayleigh number. In particular, a so-called ultimate regime has been proposed in which the heat transport becomes independent of the diffusivity and viscosity (Kraichnan 1962; Spiegel 1971), much as the energy dissipation in three-dimensional turbulence becomes independent of viscosity at high Reynolds numbers. However, evidence that an ultimate regime exists in the standard problem is mixed, even at very high Rayleigh number (Ahlers *et al.* 2009) and in some configurations the ultimate regime provably cannot exist (Whitehead & Doering 2011). One is left with the somewhat uncomfortable notion that the heat transport in Rayleigh–Bénard convection may always depend on molecular properties, no matter how turbulent the flow. The fundamental difference in this regard between Rayleigh–Bénard convection and homogeneous turbulence stems from the fact that the buoyancy must enter the fluid through a thin boundary layer in which diffusivity is unavoidably important. If in numerical experiments one eliminates the boundary layer by making the flow periodic in the vertical (Lohse & Toschi 2003), or if in laboratory experiments one breaks the boundary layer by making the surface rough (Roche *et al.* 2001), then an ultimate state for those systems may emerge.

As fundamental and important as these matters are, progress in the theory of atmospheric convection has, with a few exceptions, proceeded largely independently of them. One reason for this is that Earth's atmosphere contains a condensate, water. A wet lower surface provides a moisture source, and when the water vapour condenses heat is released, enhancing the convection. The consequences of this are considerable, with the most apparent being that the critical lapse rate for convection is no longer

https://doi.org/10.1017/jfm.2018.954 Published online by Cambridge University Press

simply that corresponding to a vertical buoyancy (or potential temperature) gradient of zero (neglecting viscous and diffusive effects); rather, a profile that is stable when dry may be unstable when saturated (e.g. Emanuel 1994; Ambaum 2010). The 'saturated adiabatic lapse rate' gives this critical lapse rate, which in the Earth's atmosphere varies between approximately 3° km^{-1} and 9.8° km^{-1}, whereas the 'dry adiabatic lapse rate' for an ideal gas is given by g/c_p and is 9.8° km^{-1} on Earth corresponding to zero vertical gradient of potential temperature (which is a proxy for buoyancy). Moisture also brings with it the possibility of conditional instability. Here, a fluid parcel containing moisture may be stable to small perturbations, but if the parcel is lifted and the water vapour condenses, the release of latent heat may then be sufficient to destabilize the fluid. Furthermore, after condensation the water droplets may stay suspended as a cloud (affecting the radiation budget), or freeze to form ice, or the moisture may fall as rain. The rain drops may partially re-evaporate before reaching the ground, leading to 'cold pools' – regions of evaporatively cooled air that reach the surface and then spread out as density currents (e.g. Tompkins 2001), and which are sometimes regarded as key ingredients in convective organization. A great many types of behaviour have been seen – including clustering and aggregation and other patterns. Moisture is not essential to organized behaviour, since various patterns occur in dry Rayleigh–Bénard convection (Golubitsky, Swift & Knobloch 1984; Cross & Hohenberg 1993), but is likely important in determining the nature of the organization.

Although the presence of condensation is the main difference between Rayleigh–Bénard convection and atmospheric convection, it is not the only one. Rayleigh–Bénard convection is, by tradition, dry, uses a Boussinesq fluid between two plates, and diffusion of heat from the boundaries provides the only source and sink of buoyancy. As well as being (frequently) moist, atmospheric convection occurs in an ideal gas, has no upper boundary and radiation provides another source of buoyancy – both heating the fluid near the ground and, perhaps more significantly, cooling the fluid internally. The radiative cooling brings an up–down asymmetry (Parodi, Emanuel & Provenzale 2003; Berlengiero *et al.* 2012) that may be as significant as moisture itself in so doing, and may be at least partially responsible for removing the bottleneck of molecular diffusivity in the boundary. Shear-induced turbulence at the lower boundary is also likely important in this regard. These various complications have led to theories of atmospheric convection becoming separated from the theories of Rayleigh–Bénard convection, with respect to both boundary layers and deep convection. For example, the similarity theory of Monin & Obukhov (1954) has provided a very well-verified foundation for parametrizations of the atmospheric boundary layer in some conditions, and it makes no reference to molecular values at all. It does, however, make reference to a roughness length and a 'Monin–Obukhov' length to take into account buoyancy effects. This remarkably useful theory in the field has found little direct application in laboratory studies in which the free convective limit is the main interest, but it does point to the importance of surface roughness, and indeed laboratory experiments almost always find that the Nusselt number increases with roughness (Chillà & Schumacher 2012). Thus, although the two fields may be disjoint, they are not in contradiction.

Away from the boundary layer, theories of atmospheric convection have tended to draw more on plume theories and (more global in nature) quasi-equilibrium ideas (e.g. Emanuel, Neelin & Bretherton 1994) that have their origins in Scorer & Ludlam (1953), Morton, Taylor & Turner (1956) and Ludlam (1966), whereas theories of Rayleigh–Bénard turbulence tend to be more statistically based and/or seek scaling

https://doi.org/10.1017/jfm.2018.954 Published online by Cambridge University Press

relations (Kraichnan, *op. cit.*, Grossmann & Lohse 2000). The numerical models used in atmospheric convection also vary widely, with different choices of microphysics, radiation schemes and resolution – with the resolution being far from that needed to use molecular values of viscosity and diffusion, or even from resolving the cloud plumes (e.g. Bryan, Wyngaard & Fritsch 2003, and true today). Various eddy viscosity and subgrid parametrization schemes are perforce used for both the free atmosphere and the boundary layer (e.g. Smagorinsky (1963), Mellor & Yamada (1974) and k–ϵ models) and depending on the resolution and choices used the models may be labelled large-eddy models or cloud resolving models. The parameters that are known to be important in Rayleigh–Bénard convection, specifically the Rayleigh number and the Prandtl number, then play no direct role in most theories (or numerical models) of atmospheric convection, and the differences between the various models often make it difficult to know whether the behaviour seen in a particular case (e.g. convective aggregation) but not in another is a true effect or an artefact of a particular model. The consequence is that reproducibility is difficult to achieve unless the numerical code itself is duplicated, and model intercomparison projects are used to compare models. In some contrast, the transition to turbulence and indeed some of the turbulent properties themselves of dry Rayleigh–Bénard convection are now fairly well modelled.

However, dry Rayleigh–Bénard convection is of itself a poor model of atmospheric convection, because the simplifications of the model become oversimplifications in an atmospheric context. It is one of the purposes of this paper to help bridge the gap between a simple but not directly relevant model (the Rayleigh–Bénard one) and complex cloud resolving models with less well understood behaviour. Along these lines, Emanuel (1994) begins his book on atmospheric convection with a discussion of plumes and the Rayleigh–Bénard problem, and Bretherton (1987, 1988), Spyksma, Bartello & Yau (2006), and Pauluis & Schumacher (2010) and Schumacher & Pauluis (2010) all make links between the two systems. Bretherton was interested in the properties of non-precipitating convection and included liquid water in a fluid contained between two plates. Spyksma *et al.* (2006) performed bubble simulations with a similar model, implemented in a triply periodic domain. Pauluis and Schumacher also kept liquid water and used a piecewise linear equation of state in which the buoyancy derivatives depend only on whether a parcel is saturated or not. Precipitating convection was the object of the idealized study by Hernandez-Duenas *et al.* (2013), who presented a model in which water vapour converted to rain water that fell and potentially re-evaporated. A number of studies have also examined the problem of two-phase Rayleigh–Bénard convection, for example when a fluid boils (Schmidt *et al.* 2011; Lakkaraju *et al.* 2013) or in mantle convection (Christensen 1995). Note that no system enables one to model a turbulent convection problem in a realistic geophysical or astrophysical setting using molecular values for diffusion and viscosity.

In this paper our goals are to present a model that represents an essence of moist convection, in order that the system may be explored at a fundamental level, and to begin to study that model. We do this by adding a single, active, condensate to the Rayleigh–Bénard model; all the condensate is removed immediately on saturation (there is no liquid phase), so providing a buoyancy source, and diffusion from the lower boundary replenishes the humidity. This 'Rainy–Bénard' model is thus relatively simple (in construct, if not behaviour) and is wholly reproducible. It should be recognized, though, that this model is not directly representative of atmospheric convection in which the buoyancy fluxes are thought not to be limited by the

https://doi.org/10.1017/jfm.2018.954 Published online by Cambridge University Press

molecular diffusivities at the boundaries, and where re-evaporation can be important. We begin, in § 2, with the equations of motion and then, in §§ 3 and 4, discuss the system's thermodynamic properties and the non-dimensional parameters that govern it. In § 5 we derive the drizzle solution, a state of no motion in which diffusion of moisture and buoyancy is exactly balanced by condensation and its release of latent heat, and which is the moist extension of the conductive state of Rayleigh–Bénard convection. We explore the stability properties of that state and then, in § 6, we describe some numerical solutions of the full, nonlinear and generally time-dependent, system. Finally, in § 7, we conclude and discuss a pathway to more realism.

2. The model

2.1. *Dry equations of motion*

We first derive a set of dry Boussinesq ideal-gas equations. Our equations may be derived by adding an incompressibility ansatz to the anelastic equations found in Vallis (2017), and a similar set of equations was presented by Spiegel & Veronis (1960) and discussed by Mahrt (1986). However, as we need to keep explicit track of both potential temperature and temperature for the moist extension, it is more transparent to proceed *ab initio*. The main assumptions are that the perturbation density is smaller than the basic-state density and that the temperature profile of the basic state is nearly adiabatic. We consider a Cartesian domain with z the vertical coordinate and write

$$\rho = \rho_0 + \delta\rho, \quad p = p_0(z) + \delta p, \tag{2.1a,b}$$

where ρ is density, p is pressure, ρ_0 is a constant, $\mathrm{d}p_0/\mathrm{d}z \equiv -\rho_0 g$ and $|\delta\rho| \ll \rho_0$, which is the fundamental Boussinesq ansatz. The momentum equations may then be written in the Boussinesq approximation as

$$\frac{\mathrm{D}\boldsymbol{u}}{\mathrm{D}t} = -\nabla\phi + \nu\nabla^2\boldsymbol{u}, \tag{2.2a}$$

$$\frac{\mathrm{D}w}{\mathrm{D}t} = -\frac{\partial\phi}{\partial z} + b + \nu\nabla^2 w. \tag{2.2b}$$

Here, $\boldsymbol{v} = (u, v, w)$ is the three-dimensional velocity, $\boldsymbol{u}$ is the horizontal velocity (u, v), w is the vertical velocity, $\phi = \delta p/\rho_0$ and $b = -g\delta\rho/\rho_0$ is the buoyancy. The mass conservation equation takes the incompressible form

$$\frac{\partial u}{\partial x} + \frac{\partial v}{\partial y} + \frac{\partial w}{\partial z} = 0. \tag{2.3}$$

To obtain a thermodynamic equation we begin with the first law of thermodynamics, written for an ideal gas and without approximation, as (e.g. Vallis 2017, chap. 1)

$$c_p\frac{\mathrm{D}T}{\mathrm{D}t} - \frac{1}{\rho}\frac{\mathrm{D}p}{\mathrm{D}t} = Q, \tag{2.4}$$

where Q is the heating, which includes diffusion. The second term on the left-hand side may be approximated by

$$\frac{1}{\rho}\frac{\mathrm{D}p}{\mathrm{D}t} \approx \left(\frac{w}{\rho_0}\right)\frac{\mathrm{d}p_0}{\mathrm{d}z} = -wg, \tag{2.5}$$

https://doi.org/10.1017/jfm.2018.954 Published online by Cambridge University Press

and (2.4) becomes

$$\frac{\mathrm{D}}{\mathrm{D}t}(c_pT + gz) = Q, \tag{2.6}$$

or

$$\frac{\mathrm{D}\theta}{\mathrm{D}t} = \frac{Q}{c_p}, \tag{2.7}$$

where

$$\theta \equiv T + \frac{g}{c_p}z \tag{2.8}$$

is the potential temperature for this system, and g/c_p is the 'dry adiabatic' lapse rate.

It remains to relate the buoyancy to the potential temperature. The density perturbations may be written as

$$\begin{aligned}\delta\rho &= \frac{\partial\rho}{\partial T}\delta T + \frac{\partial\rho}{\partial z}\delta z \\ &= \frac{\partial\rho}{\partial T}\delta T - \frac{\partial\rho}{\partial T}\frac{\partial T}{\partial z}\delta z.\end{aligned} \tag{2.9}$$

We now assume (in common with most derivations of anelastic equations) that deviations from a neutral profile are small and that $\partial T/\partial z \approx -g/c_p$. Equation (2.9) becomes

$$\delta\rho = \frac{\partial\rho}{\partial T}\left(\delta T + \frac{g}{c_p}\delta z\right) = -\frac{\rho}{T}\left(\delta T + \frac{g}{c_p}\delta z\right) \tag{2.10}$$

using the ideal-gas equation. Using (2.8) the right-hand side of the above is just $-\rho/T$ multiplied by the perturbation potential temperature and, since $\rho = \rho_0$ and $T = T_0$ at lowest order, we have

$$\frac{\delta\rho}{\rho_0} \approx -\frac{\delta\theta}{T_0}. \tag{2.11}$$

The complete set of equations, including viscous and diffusive terms, are then

$$\frac{\mathrm{D}\boldsymbol{v}}{\mathrm{D}t} = -\boldsymbol{\nabla}\phi + b\hat{\boldsymbol{z}} + \nu\nabla^2\boldsymbol{v}, \tag{2.12a}$$

$$\boldsymbol{\nabla}\cdot\boldsymbol{v} = \frac{\partial u}{\partial x} + \frac{\partial v}{\partial y} + \frac{\partial w}{\partial z} = 0, \tag{2.12b}$$

$$\frac{\mathrm{D}b}{\mathrm{D}t} = \kappa\nabla^2 b + Q_b, \tag{2.12c}$$

where Q_b represents the effects of non-diffusional heating on the buoyancy. These equations are identical to those of a simple Boussinesq system with a linear equation of state. The temperature is related to the buoyancy by

$$T = T_0 + \delta T = \theta_0 + \delta\theta - \frac{g}{c_p}z, \quad \text{or} \quad \delta T = \frac{\theta_0 b}{g} - \frac{g}{c_p}z, \tag{2.13a,b}$$

where $\theta_0 = T_0$ and $b = g\delta\theta/T_0$.

https://doi.org/10.1017/jfm.2018.954 Published online by Cambridge University Press

2.2. *Moist equations of motion*

Taking specific humidity q (water vapour content divided by total mass of a parcel) as a materially conserved variable, except for diffusion and condensation, we have

$$\frac{\mathrm{D}q}{\mathrm{D}t} = \kappa_q \nabla^2 q + C, \tag{2.14}$$

where evaporative effects are contained in the diffusion term and C represents condensation. We assume that condensation occurs almost immediately upon saturation, reducing the value of q to its saturated value. One may represent this process by

$$C = -\frac{q - q_s}{\tau} \mathcal{H}(q - q_s), \tag{2.15}$$

where $\mathcal{H}$ is the Heaviside function and τ is the time scale for condensation, which in the 'fast condensation limit' is smaller than any other dynamical time scale in the system. All the condensate is then assumed to disappear from the system, and no liquid water is present. We regard (2.15) as a simple representation of the condensation process and a means of avoiding complications with the uncertain microphysical processes employed in more complex models that retain the liquid and ice phases (Khain *et al.* 2015; Zhao *et al.* 2016; White *et al.* 2017). An analogous fast autoconversion process between phases is sometimes used in these types of models. Fast condensation may be regarded as a limiting form of a unary chemical reaction (Pierrehumbert, Brogniez & Roca 2007); similar equations were also used by or appeared in the theoretical studies of O'Gorman & Schneider (2006), Sukhatme & Young (2011) and Tsang & Vanneste (2017), as well as in some idealized general circulation models (e.g. Frierson, Held & Zurita-Gotor 2006), and we refer the reader to these papers for more discussion. It is by choice that we omit liquid and ice phases of water in order to make a closer connection to the Rayleigh–Bénard problem, and this is one of the ways our model differs from cloud resolving models.

The value of q_s is given by an approximation to the solution of the Clausius–Clapeyron equation for an ideal gas, as follows. If the latent heat of condensation, L, is constant (in actuality L for water varies by approximately 10 % between 0 °C and 100 °C) then the saturation vapour pressure, e_s, is given by

$$e_s = e_0 \exp\left[\frac{L}{R_v}\left(\frac{1}{T_0} - \frac{1}{T}\right)\right], \tag{2.16}$$

where R_v is the gas constant for water vapour and e_0 and T_0 are constants. For small variations in absolute temperature (2.16) approximates to

$$e_s = e_0 \exp\left(\frac{L(T - T_0)}{R_v T_0^2}\right) = e_0 \exp(\alpha \delta T), \tag{2.17}$$

where $\alpha = L/(R_v T_0^2)$ and $\delta T = T - T_0$.

The specific humidity is related to the vapour pressure, e, by

$$q = \frac{\epsilon e}{p - e} \approx \epsilon \frac{e_s}{p}, \tag{2.18}$$

where ϵ is the ratio of the molar mass of water vapour (or other condensate) to that of dry air and is approximately 0.62 for water and air. The approximation that $p \gg e$ is normally a very good one for Earth's atmosphere.

https://doi.org/10.1017/jfm.2018.954 Published online by Cambridge University Press

The lowest-order approximation to pressure in (2.18) is to take $p = p_0$ so that

$$q_s = q_0 \exp(\alpha \delta T), \tag{2.19}$$

where $q_0 = \epsilon e_0 / p_0$ is the value of the saturation specific humidity when $\delta T = 0$. More accurately we may write

$$p = p_0 \left(\frac{T}{\theta} \right)^{c_p/R_d} \approx p_0 \left(\frac{T}{\theta_0} \right)^{c_p/R_d}, \tag{2.20}$$

assuming that $\theta \approx \theta_0$, and where R_d is the gas constant of dry air. If we expand T about a reference state, T_0, then a little manipulation leads to

$$p = p_0 \exp \left(\frac{c_p \delta T}{R_d T_0} \right), \tag{2.21}$$

and thence, using (2.17) and (2.18), to

$$q_s = q_0 \exp(\alpha' \delta T), \tag{2.22}$$

where $\alpha' = \alpha - c_p/(R_d T_0) = L/(R_v T_0^2) - c_p/(R_d T_0)$. This relation has the same form as (2.19) and we henceforth drop the prime on α. For water vapour, $L/(R_v T_0^2)$ is approximately three times larger than $c_p/(R_d T_0)$ at 273 K. We refer to (2.22) and similar equations as Clausius–Clapeyron relations, and we henceforth refer to δT as T.

The condensation of moisture provides a buoyancy source that can be determined from the first law of thermodynamics

$$L \Delta q = c_p \Delta T = \frac{c_p \theta_0}{g} \Delta b, \tag{2.23}$$

or

$$\gamma \, \Delta q = \Delta b, \tag{2.24}$$

where $\gamma = gL/(c_p \theta_0)$ is a constant, so providing a non-zero Q_b term on the right-hand side of the buoyancy equation (2.12*c*).

2.3. *Dimensional equations*

The full, dimensional, equations of motion are as follows:

$$\frac{\mathrm{D}\boldsymbol{u}}{\mathrm{D}t} = -\boldsymbol{\nabla}\phi + \nu \nabla^2 \boldsymbol{u}, \tag{2.25a}$$

$$\frac{\mathrm{D}w}{\mathrm{D}t} = -\frac{\partial \phi}{\partial z} + b + \nu \nabla^2 w, \tag{2.25b}$$

$$\frac{\mathrm{D}b}{\mathrm{D}t} = \gamma \frac{q - q_s}{\tau} \mathcal{H}(q - q_s) + \kappa \nabla^2 b, \tag{2.25c}$$

$$\frac{\mathrm{D}q}{\mathrm{D}t} = -\frac{q - q_s}{\tau} \mathcal{H}(q - q_s) + \kappa_q \nabla^2 q, \tag{2.25d}$$

$$\boldsymbol{\nabla} \cdot \boldsymbol{v} \equiv \left(\frac{\partial u}{\partial x} + \frac{\partial v}{\partial y} + \frac{\partial w}{\partial z} \right) = 0. \tag{2.25e}$$

https://doi.org/10.1017/jfm.2018.954 Published online by Cambridge University Press

The temperature is obtained from the buoyancy by

$$T = \frac{\theta_0}{g} b - \frac{gz}{c_p} \tag{2.25f}$$

and the saturation humidity is given by

$$q_s = q_0 \mathrm{e}^{\alpha T}, \tag{2.25g}$$

where q_0 and α are constants. The buoyancy here is not a function of the amount of water vapour in the system, which is appropriate if the system is sufficiently dilute. (Meteorologists account for this by use of a 'virtual temperature', but here we ignore that effect.) A useful measure of the degree of saturation of a parcel is the relative humidity, r, which here we define as $r = q/q_s(T)$.

The only difference from the standard Boussinesq Rayleigh–Bénard equations is the presence of the moisture term, and because q_s is a function of absolute temperature (not buoyancy), it is necessary to keep track of the local temperature via (2.25*f*). The moisture term can be expected to be particularly important in updraughts: air that is rising will cool, become saturated and condense, releasing heat and increasing the buoyancy. On the other hand, descending air becomes warmer and less saturated and (absent diabatic effects) parcels typically follow the dry adiabatic lapse rate.

The system (2.25*a–g*) is a closed set of dimensional equations that need to be supplemented by boundary conditions on the variables. In this paper we take the variables to be periodic in the horizontal and generally impose no-slip, fixed temperature (and hence fixed buoyancy) and fixed specific humidity on the horizontal boundaries. If we set the specific humidity to be at its saturated value at the top and bottom boundary then typical boundary conditions are

$$b(z=0) = 0, \quad b(z=H) = -\Delta b, \tag{2.26a,b}$$

$$T(z=0) = 0, \quad T(z=H) = T_2, \tag{2.26c,d}$$

$$q(z=0) = q_0, \quad q(z=H) = q_s(T_2), \tag{2.26e,f}$$

where H is the top of the domain and $T_2 = -\Delta b(\theta_0/g) - gH/c_p$. Alternatively, one might set $\partial q/\partial z = 0$ at the top boundary, so that there is no source or sink of humidity at the top.

Of the models mentioned in the introduction, the above system differs from the non-precipitating models of Bretherton (1987) and Pauluis & Schumacher (2010) in its treatment of condensation and the equation of state – in our model water vapour is almost immediately removed from the system once saturation is reached, and consequently clouds in the usual sense do not form. Our system has some similarities with the precipitating system of Hernandez-Duenas *et al.* (2013), but it is still simpler for we do not retain liquid water. We also retain a temperature dependence in the Clausius–Clapeyron relation (in the Hernandez-Duenas system the saturated vapour pressure is just a function of height), and this is important both for the drizzle solution of § 5 and for the nonlinear, time-dependent solutions.

3. Thermodynamic and conservation properties

3.1. *Moist static energy and saturated lapse rate*

From (2.25*c*) and (2.25*d*) we obtain

$$\frac{\mathrm{D}m}{\mathrm{D}t} = \kappa \nabla^2 b + \gamma \kappa_q \nabla^2 q, \tag{3.1a}$$

where

$$m = b + \gamma q. \tag{3.1b}$$

https://doi.org/10.1017/jfm.2018.954 Published online by Cambridge University Press

In the absence of diffusion the quantity m is conserved on parcels, even in the presence of condensation, and is akin to a 'moist static energy' for this system. If we integrate over volume and time then, in a statistically steady state,

$$\int \kappa \boldsymbol{\nabla} b \cdot \mathrm{d}\boldsymbol{\ell} = -\int \gamma \kappa_q \boldsymbol{\nabla} q \cdot \mathrm{d}\boldsymbol{\ell}, \tag{3.2}$$

where the integral is over the boundary. If there is condensation in the interior then there a buoyancy source in the interior, and there must be a buoyancy loss at the boundaries that balances the buoyancy gain due to condensation. The loss of water due to condensation is balanced by moisture diffusion at the boundary, and (3.2) represents the balance between buoyancy loss and moisture gain at the boundaries.

The lapse rate, $-\partial T/\partial z$, corresponding to $\partial m/\partial z = 0$ with $q = q_s$, is the so-called saturated adiabatic lapse rate, Γ_T for this system, and this is easily calculated. Using the definition of b and γ, the state of $\partial m/\partial z = 0$ corresponds to

$$\frac{\partial T}{\partial z} + \frac{g}{c_p} + \frac{L}{c_p}\frac{\partial q_s}{\partial T} = 0. \tag{3.3}$$

Using the simplified Clausius–Clapeyron relation, equation (2.25*g*), we obtain

$$\Gamma_T = \frac{g/c_p}{1 + L\alpha q_s/c_p} = \frac{g/c_p}{1 + \alpha q_s \gamma \theta_0/g}. \tag{3.4}$$

We can also write this as a critical buoyancy gradient, $\Gamma_b = \partial b/\partial z$, in which case we obtain

$$\Gamma_b = \left(\frac{g}{\theta_0}\right)\left[\frac{\partial T}{\partial z} + \frac{g}{c_p}\right] = \left[\frac{q_s \gamma \alpha g/c_p}{1 + q_s \gamma \alpha \theta_0/g}\right]. \tag{3.5}$$

If $\gamma = 0$, or if the air is not saturated, then at criticality $\Gamma_b = 0$, as expected, but otherwise Γ_b is a positive quantity. That is, the critical buoyancy lapse rate for convection is positive, and a gradient less than that of (3.5) will be unstable (in the absence of diffusion) if the air is saturated.

3.2. *Energy, potential vorticity and boundary fluxes*

If the latent heat of condensation is zero (i.e. if $\gamma = 0$) the momentum and buoyancy equations reduce to the conventional Boussinesq equations, and the moisture is just a passive scalar. In the absence of viscosity and diffusion it is well known that the equations then conserve volume integrated energy, $\int (\boldsymbol{v}^2/2 - bz)\,\mathrm{d}V$. They also conserve potential vorticity on parcels – meaning that $\mathrm{D}Q/\mathrm{D}t = 0$ where $Q = \boldsymbol{\omega} \cdot \boldsymbol{\nabla} b$, because the buoyancy term in the momentum equation is a function only of the advected variable b itself. In the full moist ideal-gas equations potential vorticity is not conserved because then the potential temperature is a function of moisture content as well as density and pressure and therefore cannot annihilate the solenoidal term (Schubert *et al.* 2001; Vallis 2017).

Neither energy nor potential vorticity are conserved in the fluid interior in the presence of condensation. The energy equation has a condensational source and is

$$\frac{\mathrm{D}}{\mathrm{D}t}\left(\frac{1}{2}\boldsymbol{v}^2 - bz\right) = -z(Q_b + Q_d) - \epsilon, \tag{3.6}$$

where $Q_b = (\gamma(q - q_s)/\tau)\mathcal{H}(q - q_s)$ is the heating due to moisture condensation (the first term on the right-hand side of (2.25*c*)), $Q_d = \kappa \nabla^2 b$, and ϵ is the kinetic-energy

https://doi.org/10.1017/jfm.2018.954 Published online by Cambridge University Press

dissipation. In a statistically steady state the left-hand side vanishes when integrated over the domain and

$$\langle z(Q_b + Q_d)\rangle = -\langle \epsilon \rangle. \tag{3.7}$$

Since the right-hand side is negative definite, the total heating, $(Q_b + Q_d)$, must be negatively correlated with the height, a known result (Paparella & Young 2002). Or, put informally, the heating must be below the cooling if kinetic energy is to be dissipated. The consequence of this is that, with periodic horizontal boundary conditions and a kinetic-energy dissipating flow, diffusion must carry buoyancy out of the fluid at the top boundary.

Finally, we note that in statistically steady state the total precipitation (namely the volume integral of the first term on the right-hand side of (2.25*d*) is (rather obviously) exactly balanced by moisture fluxes at the boundary. From (2.25*c*) the precipitation is also related to the boundary buoyancy fluxes. This type of result can provide constraints on how precipitation can evolve under climate change (e.g. O'Gorman *et al.* 2012), although we do not explore that issue here.

4. Non-dimensionalization

4.1. *Diffusive scaling*

Here we non-dimensionalize the system using the diffusivity and the height of the domain to define a time scale, as is common in Rayleigh–Bénard convection problems. In appendix A we present two other ways of proceeding, using buoyancy and moisture to provide time scales. We scale all lengths x, y, z with H, the depth of the domain, and we scale q with q_0. The thermal diffusion time, H^2/κ, then scales time, and velocity scales as κ/H. We scale pressure with velocity squared, though in the Boussinesq formulation pressure is a Lagrange multiplier to ensure incompressibility and need not directly enter the dynamics. We have a choice for scaling typical temperatures and buoyancy variables, either with the temperature or buoyancy drop across the layer, and because we shall investigate atmospheres which are stable (or marginally stable) to dry convection (so sometimes the buoyancy drop is zero) it is more useful to select the non-dimensionalization with temperature drop. Thus, with hats denoting non-dimensional variables and either an uppercase or a subscript S or 0 denoting scaling values, we choose time (t_s), velocity (U, W), buoyancy (B), moisture (Q) and pressure (Φ) scales as, respectively,

$$\left.\begin{gathered} t_S = H^2\kappa, \quad U = W = \kappa/H, \quad B = g\Delta T/\theta_0, \\ Q = q_0, \quad \Phi = U^2 = (\kappa/H)^2, \end{gathered}\right\} \tag{4.1}$$

where ΔT is the temperature difference between bottom and top. The various variable may then be written as

$$\left.\begin{gathered} (x, y, z) = (\widehat{x}, \widehat{y}, \widehat{z})H, \quad (u, v, w) = (\widehat{u}, \widehat{v}, \widehat{w})\kappa/H, \\ b = \widehat{b}\frac{g\Delta T}{\theta_0}, \quad T = \widehat{T}\Delta T, \quad q = \widehat{q}q_0, \quad m = \widehat{m}\frac{g\Delta T}{\theta_0}. \end{gathered}\right\} \tag{4.2}$$

We also define $\widehat{\tau} = \tau\kappa/H^2$ to be the condensation time in units of the thermal diffusion time. With these choices the momentum equations become

$$\frac{\mathrm{D}\widehat{\boldsymbol{u}}}{\mathrm{D}\widehat{t}} = -\boldsymbol{\nabla}\widehat{\phi} + Pr\nabla^2\widehat{\boldsymbol{u}}, \tag{4.3}$$

$$\frac{\mathrm{D}\widehat{w}}{\mathrm{D}\widehat{t}} = -\frac{\partial\widehat{\phi}}{\partial\widehat{z}} + PrRa\,\widehat{b} + Pr\nabla^2\widehat{w}. \tag{4.4}$$

https://doi.org/10.1017/jfm.2018.954 Published online by Cambridge University Press

The buoyancy and moisture equations may be written as

$$\frac{\mathrm{D}\widehat{b}}{\mathrm{D}\widehat{t}} = \widehat{\gamma}\frac{\widehat{q}-\widehat{q}_s}{\widehat{\tau}}\mathcal{H}(\widehat{q}-\widehat{q}_s) + \nabla^2\widehat{b}, \tag{4.5}$$

$$\frac{\mathrm{D}\widehat{q}}{\mathrm{D}t} = \frac{\widehat{q}_s-\widehat{q}}{\widehat{\tau}}\mathcal{H}(\widehat{q}-\widehat{q}_s) + S_m\nabla^2\widehat{q}. \tag{4.6}$$

The non-dimensional numbers are

$$Ra = \frac{\Delta T g H^3}{\theta_0 \kappa \nu}, \quad Pr = \frac{\nu}{\kappa}, \quad S_m = \frac{\kappa_q}{\kappa}, \quad \widehat{\gamma} = \gamma\left(\frac{q_0\theta_0}{g\Delta T}\right) = \frac{Lq_0}{c_p\Delta T}. \tag{4.7a–d}$$

Here, Ra is the familiar Rayleigh number, Pr is the Prandtl number, S_m is a ratio of diffusivities and $\widehat{\gamma}$ is the non-dimensional value of γ, which in turn is a measure of the importance of the latent heat of condensation. The non-dimensional moist static energy is given by $\widehat{m} = \widehat{b} + \widehat{\gamma}\widehat{q}$.

The 'physics' equations are

$$q_s = q_0\exp(\alpha T), \quad T = \frac{\theta_0}{g}b - \frac{g}{c_p}z. \tag{4.8a,b}$$

With the above non-dimensionalization these equations become

$$\widehat{q}_s = \exp(\widehat{\alpha}\widehat{T}), \quad \widehat{T} = \widehat{b} - \widehat{\beta}\widehat{z}, \tag{4.9a,b}$$

where

$$\widehat{\alpha} = \alpha\Delta T = \frac{L\Delta T}{R_v T_0^2}, \quad \widehat{\beta} = \frac{gH}{c_p\Delta T}. \tag{4.10a,b}$$

Two other ways to non-dimensionalize the system are given in appendix A, one using the buoyancy difference across the layer to scale time, and the other using the buoyancy created by condensation to scale time. The non-dimensional numbers that arise are combinations of those above, and we just note one of them here, the condensational Rayleigh number:

$$R_\gamma = \frac{gLH^3q_0}{c_p\theta_0\kappa\nu} = Ra\left(\frac{q_0L}{\Delta T c_p}\right) = Ra\widehat{\gamma}. \tag{4.11}$$

4.2. *Non-dimensional lapse rates*

The non-dimensional dry adiabatic lapse rate is given by

$$\widehat{\Gamma}_d = \frac{g}{c_p}\frac{\Delta T}{g} = \widehat{\beta}, \tag{4.12}$$

consistent with (4.9*b*). The non-dimensional saturated adiabatic lapse rate for temperature is given by

$$\widehat{\Gamma}_T = \frac{\Delta T}{g}\frac{g/c_p}{1+L\alpha q_s/c_p} = \frac{\widehat{\beta}}{1+\widehat{\gamma}\widehat{\alpha}\widehat{q}_s}, \tag{4.13}$$

https://doi.org/10.1017/jfm.2018.954 Published online by Cambridge University Press

and the corresponding lapse rate for buoyancy is given by

$$\widehat{\Gamma}_b = \frac{M\widehat{\beta}\widehat{\alpha}\widehat{q}_s}{1+\widehat{\gamma}\widehat{\alpha}\widehat{q}_s}. \tag{4.14}$$

The deviation from the dry values is proportional to the product $\widehat{\gamma}\widehat{\alpha}$, which is roughly proportional to the square of the latent heat of vaporization.

4.3. *Parameter values*

Aside from the ratio of the moisture diffusivity to the viscosity or thermal diffusivity, the new non-dimensional numbers in the system (compared to the Rayleigh–Bénard model) are as follows.

(i) The parameter $\widehat{\gamma}$ is the ratio of the buoyancy effect due to the heat release by condensation to the dry effect, namely $\widehat{\gamma} = Lq_0/(c_p\Delta T)$. The condensation Rayleigh number, $R_\gamma = gLH^3q_0/(c_p\theta_0\kappa\nu)$, captures the same effect and $\widehat{\gamma} = R_\gamma/Ra$.

(ii) The dry adiabatic lapse rate, $\widehat{\beta} = gH/(c_p\Delta T)$, derived from the dimensional value g/c_p.

(iii) The parameter $\widehat{\alpha}$ determining the exponential growth of saturation specific humidity, $\widehat{\alpha} = L\Delta T/(R_vT_0^2)$. The corresponding dimensional parameter is $L/(R_vT_o^2)$.

In Earth's atmosphere approximate dimensional values are $L = 2.5\times10^6$ J kg^{-1}, $c_p = 1004$ J kg^{-1} K^{-1}, $c_p = 718$ J kg^{-1} K^{-1}, $R = 287$ J kg^{-1} K^{-1}, $R_v = 462$ J kg^{-1} K^{-1}, $\epsilon = R_d/R = 0.622$, $e_0 = 611$ Pa, $p_0 = 10^5$ Pa, $q_0 = \epsilon e_0/p_0 = 3.8\times10^{-3}$, $H = 10^4$ m, $\Delta T = 50$ K, $g = 9.8$ m s^{-2}, $\theta_0 = 300$ K, $B = g\Delta T/\theta_0 \approx 1.6$ m^2 s^{-2}, $\nu = 1.5\times10^{-5}$ m^2 s^{-1}, $\kappa = 2.1\times10^{-5}$ m^2 s^{-1}, $\kappa_q = 2.8\times10^{-5}$ m^2 s^{-1}. Typical values of the non-dimensional parameters are then

$$Pr = \frac{\nu}{\kappa} \approx 0.7, \quad Ra = \frac{g\Delta TH^3}{\theta_0\nu\kappa} \approx 5.4\times10^{21}, \quad R_\gamma = \frac{gLH^3q_0}{(c_p\theta_0\kappa\nu)} \approx 1.0\times10^{21}, \tag{4.15a–c}$$

$$\widehat{\gamma} = \frac{Lq_0}{c_p\Delta T} = \frac{R_\gamma}{Ra} \approx 0.19, \quad \widehat{\alpha} = \frac{L\Delta T}{R_vT_0^2} \approx 3.0, \quad \widehat{\beta} = \frac{gH}{(c_p\Delta T)} \approx 1.95. \tag{4.16a–c}$$

Apart from the Rayleigh numbers these quantities are all of order unity in Earth's atmosphere. The fact that $\widehat{\gamma} \sim 1$ means that water condensation is, roughly, as important a source of buoyancy as is the temperature gradient between the ground and the tropopause (which ultimately comes from radiation). As $\widehat{\alpha} \sim 1$ the water vapour content falls off significantly over the depth of the domain. Because $\widehat{\gamma}\widehat{\alpha} \sim 1$ the moist adiabatic lapse rate is typically noticeably less than the dry adiabatic lapse rate (and detailed calculations indicate it varies by a factor of 0.3 to 1.0 of the dry adiabatic lapse rate). The fact that $\widehat{\beta} \sim 1$ indicates that temperature significantly differs from potential temperature over the depth of the troposphere, but is of the same order of magnitude.

For comparison, consider also the values for Jupiter and Titan, two other atmospheres with condensates in the Solar System. On Jupiter water vapour is a condensate but the predominant gas is hydrogen (so that ϵ and the heat

https://doi.org/10.1017/jfm.2018.954 Published online by Cambridge University Press

capacities differ), and gravity is larger. In Jupiter's weather layer (at a pressure of 3 bars, say) we might take $c_p = 1.4\times10^4$ J kg^{-1} K^{-1}, $H = 100$ km, $p_0 = 3\times10^5$ Pa, $g = 50$ m s^{-2}, $\epsilon = 9$, $q_0 = \epsilon e_0/p_0 = 1.8\times10^{-2}$, $\Delta T = 100$ K, giving $\widehat{\gamma} = 0.03$ and $\widehat{\alpha} = 6$. The value of $\widehat{\gamma}$ is smaller than that for Earth because of the higher value of pressure chosen (3 bars instead of 1), and the larger temperature difference suggesting that water condensation is not a primary factor over the whole Jovian troposphere (meaning the weather layer below the stratosphere), but may still be important in the lower troposphere. The value of $\widehat{\gamma}\widehat{\alpha}$ is approximately 0.2, indicating a moist adiabatic lapse rate somewhat less than the dry one, but not significantly so. The value of $\widehat{\beta}$ is approximately 3.6 (for $H = 100$ km) indicating that the temperature differs from the potential temperature over the depth of the troposphere.

On Titan, which has a surface temperature of approximately 100 K, nitrogen is the main component of the dry atmosphere and methane is the main condensate, with concentrations varying between approximately 1 and 5 %. The latent heat of condensation for methane is $L \approx 4.8\times10^5$ J kg^{-1} and its gas constant is $R_v = 518$ J kg^{-1} K^{-1}. The heat capacity of its nitrogen atmosphere is about the same as air on Earth so that $c_p \approx 10^3$ J kg-1 K^{-1}, and $g \approx 1.35$ m s^{-2} and there is an estimated temperature drop of approximately 25 K over a tropospheric depth of 40 km, with a surface pressure of roughly 10^5 Pa, and a representative value of q_0 for methane is 10^{-2}. Typical values are then $\widehat{\gamma} = 0.2$, $\widehat{\alpha} = 2.3$, not dissimilar to those for Earth, suggesting that condensation is an important source of buoyancy and that the moist adiabatic lapse rate will be noticeably smaller than the dry one, as detailed calculations confirm (Mitchell & Lora 2016). We also find $\widehat{\beta} = 1.6$, similar to Earth's value.

4.4. *A note on parameter independence and thermodynamic consistency*

The non-dimensional parameters $\widehat{\gamma}, \widehat{\alpha}$ and $\widehat{\beta}$ contain different combinations of various physical constants. This means that, even though L appears in both $\widehat{\gamma}$ and $\widehat{\alpha}$, and c_p appears in both $\widehat{\gamma}$ and $\widehat{\beta}$, the values of the non-dimensional parameters may be varied independently without thermodynamic inconsistency. The value of L is related to the difference in the heat capacities of the condensate in its liquid and vapour forms, c_p^l and c_p^v respectively, but this is not the only factor determining L. (To a good approximation, $L = L_0 + (c_p^v - c_p^l)T$, but the L_0 term usually dominates and so L is almost constant and independent of the heat capacity of the condensate.) Thus, although the gas constant of the vapour, R_v, does appear in the expression for $\widehat{\alpha}$ along with L, $\widehat{\alpha}$ is effectively an independent parameter, meaning that it may be varied independently of $\widehat{\gamma}$ (and of $\widehat{\beta}$). Varying the parameters does imply a variation in the physical nature of the condensate and the dry air, and, for example, if one wished to explore the effect of a reduction of the latent heat alone one would need to change $\widehat{\gamma}$ and $\widehat{\alpha}$ consistently. If one wished to transition continuously to the dry system then a simple way would be to take $\widehat{\gamma} \to 0$ and $\widehat{\alpha} \to 0$, noting that $\widehat{\alpha}$ has no effect when $\widehat{\gamma} = 0$.

In the rest of the paper we drop the hats on the non-dimensional variables and the dimensional/non-dimensional distinction will be apparent by context. Also, unless explicitly noted, we take $Pr = S_m = 1$ and we take τ (formerly $\widehat{\tau}$) to be 5×10^{-5}.

5. The drizzle solution

The classical Rayleigh–Bénard problem has a diffusive solution of no motion and a linear gradient of buoyancy connecting the upper and lower boundaries.

https://doi.org/10.1017/jfm.2018.954 Published online by Cambridge University Press

The Rainy–Bénard problem has an analogous diffusive solution, but moisture (as well as buoyancy) now diffuses from the lower boundary, condenses and falls out as drizzle, at a rate determined by the rate of diffusion. (Meteorologists define drizzle as light precipitation with small water droplets, usually less than 0.5 mm in diameter (American Meteorological Society 2018). Here we have no droplet size, but the precipitation is very light compared to our convecting solutions.) Furthermore, the condensation occurs at saturation, and the temperature, and hence the value of the saturation humidity, is determined by the release of latent heat. The upshot of this is that we have a nonlinear problem even in the absence of motion, and we now find its solution.

5.1. *Saturated boundaries*

Let us calculate a time-independent basic state solution to the non-dimensional equations (4.3)–(4.6), together with the physics equations, (4.9). In the case of no motion, horizontal homogeneity and a saturated domain the thermodynamic and moisture equations are, with $S_m = 1$ and a diffusive non-dimensionalization,

$$\frac{\mathrm{d}^2 b}{\mathrm{d}z^2} = -\gamma \frac{q - q_s}{\tau}, \tag{5.1a}$$

$$\frac{\mathrm{d}^2 q}{\mathrm{d}z^2} = \frac{q - q_s}{\tau}. \tag{5.1b}$$

Evidently there is a solution of the moist static energy, $m = b + \gamma q$ that obeys

$$\frac{\mathrm{d}^2 m}{\mathrm{d}z^2} = 0, \tag{5.2}$$

yielding a linear dependence of m with height, i.e. $m = P + Qz$, regardless of the presence or otherwise of condensation, where the constants P and Q are determined by the boundary conditions. If we specify that $b = b_1$ and $b = b_2$ at the lower and upper boundaries, respectively, or equivalently $T_1 = b_1$ and $T_2 = b_2 - \beta$, and that these boundaries are saturated with values q_1 and q_2 respectively, then, at $z = 0$,

$$P = b_1 + \gamma q_1 = T_1 + \gamma q_1 = T_1 + \gamma \exp(\alpha T_1). \tag{5.3}$$

At the top, $z = 1$, we have $b_2 + \gamma q_2 = P + Q$, whence

$$Q = [(b_2 - b_1) + \gamma (q_2 - q_1)] = \beta + T_2 - T_1 + \gamma (\exp(\alpha T_2) - \exp(\alpha T_1)). \tag{5.4}$$

The solution then satisfies $b + \gamma q = P + Qz$ with P and Q as above. Now, for small τ and provided that moisture is converging everywhere, the humidity must everywhere be very close to its saturated value. That is, $q = q_s + \tau q' + O(\tau^2)$ and therefore

$$b + \gamma q_s = P + Qz + O(\tau). \tag{5.5}$$

Using the Clausius–Clapeyron relation, (4.9), for q_s then gives, for small τ,

$$P + Qz = b + \gamma \exp(\alpha(b - \beta z)), \tag{5.6}$$

or equivalently

$$P + Qz = T + \beta z + \gamma \exp(\alpha T). \tag{5.7}$$

https://doi.org/10.1017/jfm.2018.954 Published online by Cambridge University Press

This algebraic equation for b or T may be solved via an iterative root-finding algorithm, or analytically by use of the Lambert-W function, which is the function that satisfies the equation $\mathrm{W}(\chi)\exp(\mathrm{W}(\chi)) = \chi$ for any χ. Explicitly, the exact solution of (5.7) is given by

$$T(z) = C - \frac{\mathrm{W}(\alpha\gamma\exp(\alpha C))}{\alpha}, \tag{5.8}$$

where $C = P + (Q-\beta)z$ with P and Q given by (5.3) and (5.4). As soon as T is known then q_s is given using (4.8*a*). From (5.6) we also see that

$$\frac{\mathrm{d}^2 b}{\mathrm{d}z^2} = -\gamma\alpha^2\beta^2\exp(\alpha(b-\beta z)) < 0, \tag{5.9}$$

$$\frac{\mathrm{d}^2 q}{\mathrm{d}z^2} = \alpha^2\beta^2\exp(\alpha(b-\beta z)) > 0. \tag{5.10}$$

That is to say, the solution for q is convex and moisture does indeed converge to every point in the domain, meaning that the solution must be at least saturated everywhere, consistent with the assumption.

The temperature and humidity profiles do not depend on the value of the diffusivity. However, the rate of condensation (i.e. the rainfall) does. To see this explicitly we use the diffusion-based non-dimensionalization and temporarily restore the hats on non-dimensional variables. Setting the left-hand sides of (4.5) and (4.6) to zero and using $\widehat{q} = \widehat{q}_s + \widehat{\tau}\widehat{q'}$ gives

$$\widehat{\gamma}\widehat{q'} = -\frac{\mathrm{d}^2\widehat{b}}{\mathrm{d}\widehat{z}^2}, \quad \text{and} \quad \widehat{q'} = \frac{\mathrm{d}^2\widehat{q}_s}{\mathrm{d}\widehat{z}^2}. \tag{5.11a,b}$$

The dimensional value of the perturbation buoyancy, q', is obtained from

$$q' = \widehat{\tau}\widehat{q'}q_0 = \frac{\kappa}{H^2}\tau\widehat{q'}q_0, \tag{5.12}$$

so that, re-dimensionalizing (5.11*b*), we obtain

$$\frac{H^2}{\kappa q_0}\frac{q'}{\tau} = \frac{\mathrm{d}^2 q_s}{\mathrm{d}z^2}\frac{H^2}{q_0}, \quad \text{or} \quad \frac{q'}{\tau} = \kappa\frac{\mathrm{d}^2 q_s}{\mathrm{d}z^2}. \tag{5.13a,b}$$

This expression gives the condensation rate, since $\kappa\mathrm{d}^2 q_s/\mathrm{d}z^2$ is the moisture convergence. Thus, the fields of buoyancy and moisture themselves do not depend on the diffusivity but the rate of condensation does. Although this result may seem obvious from the form of the dimensional equations, it is only when $\widehat{\tau} \ll 1$ (non-dimensionally) or $\tau \ll H^2/\kappa$ (dimensionally) that it is valid, because only then is q' small and $q \approx q_s$.

Figure 1 shows various profiles for buoyancy, temperature, humidity and $m(z)$ for a typical set of non-dimensional parameters. For this set of parameters, which is stable to dry convection, the buoyancy increases with height in the lower part of the domain, but decreases slightly in the top part of the domain. The variable $m(z)$ is linearly decreasing with height, implying that the solution will be unstable to moist convection in the diffusion-free limit. Finally, we remark that, at low Rayleigh number, numerical solutions of the nonlinear, time-dependent equations do converge to the drizzle solution.

https://doi.org/10.1017/jfm.2018.954 Published online by Cambridge University Press

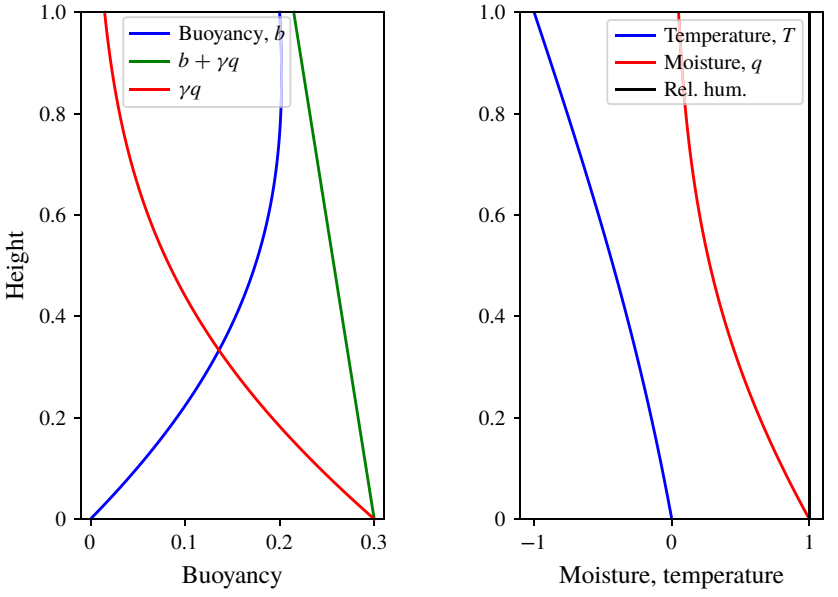


FIGURE 1. (Colour online) A non-dimensional drizzle solution with saturated upper and lower boundaries. The boundary conditions are that $b = 0$ at $z = 0$ and $b = 0.2$ at $z = 1$ and $q = q_s$ at both boundaries, thus giving the values of m $(= b + \gamma q)$ at the boundaries shown. These solutions were obtained with $\gamma = 0.3$, $\alpha = 3$ and $\beta = 1.2$.

5.1.1. *The linear drizzle problem*

The drizzle problem may be further simplified by linearizing the solution to the Clausius–Clapeyron equation, so that $q_s = (1 + \alpha T) = (1 + \alpha(b - \beta z))$, but this leads to an uninteresting case. Suppose that the boundaries are saturated, with a higher temperature at the bottom. The solution to (5.1) is then just a linear profile of both b and q between lower and upper boundaries. Although the domain is saturated everywhere there is no convergence of moisture, and no condensation, because $\mathrm{d}^2 q_s/\mathrm{d}z^2 = 0$ everywhere. The moisture content of the fluid must increase faster than linearly with temperature in order to produce condensation, as with the exponential relation (2.25g) that arises from the Clausius–Clapeyron equation.

5.2. *Drizzle solution with unsaturated boundaries*

In geophysical settings it is common to suppose that the lower boundary condition on moisture does not correspond to saturation; that is, the boundary – for example moist soil – is damp but not saturated; there will then be a layer of unsaturated air adjacent to the boundary. In the unsaturated layer the buoyancy and the moisture diffuse independently and each has a linear profile, but if the temperature falls off sufficiently rapidly with height then the water vapour will become saturated at some level, above which a solution similar to that of (5.6) holds.

Suppose that, as before, the boundary conditions at the bottom and top of the domain are (b_1, q_1) and (b_2, q_2) respectively, but that q_1 is less than the saturated value. The solution will be unsaturated below some height z_c at which condensation begins, and for $0 < z < z_c$ the profiles of both b and q are linear in z, with no condensation. At z_c the humidity takes its saturated value at z_c and therefore

https://doi.org/10.1017/jfm.2018.954 Published online by Cambridge University Press

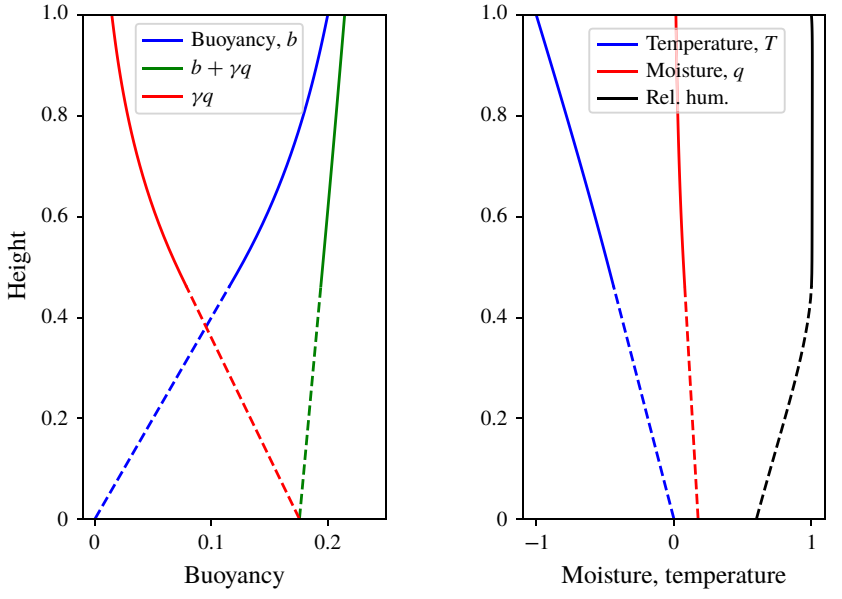


FIGURE 2. (Colour online) Drizzle solution with an unsaturated lower boundary, with relative humidity (q/q_s) of 0.5. Other parameters are the same as in figure 1. The dashed lines show the linear profiles of moisture and buoyancy up to a height of approximately 0.45, above which the solution is saturated.

$q_c = q_s(b_c) = \exp[\alpha(b_c - \beta z_c)]$. Above q_c region is completely saturated and the calculation proceeds, in principle, as in the previous subsection, but with different boundary conditions and over the smaller domain. The height z_c is determined by requiring that the first derivatives of temperature and moisture (as well as the values themselves) are continuous at the level of saturation, and this is most easily done numerically. That the first derivative should be continuous can be seen by integrating the governing equation across the condensation level giving

$$\int_{z_c-\epsilon}^{z_c+\epsilon} \kappa \frac{\partial^2 q}{\partial z^2}\, \mathrm{d}z = \int_{z_c-\epsilon}^{z_c+\epsilon} \mathcal{H}(q-q_s)\frac{(q-q_s)}{\tau}\, \mathrm{d}z. \tag{5.14}$$

The right-hand side goes to zero as $\epsilon \to 0$, even with the Heaviside function, and hence $\partial q/\partial z$ remains continuous, and similarly for temperature and buoyancy.

If the lower boundary is chosen to be saturated the solution is that described previously, whereas if the lower boundary is sufficiently dry then there is no condensation and buoyancy and moisture both vary linearly from bottom to top. A typical intermediate solution is illustrated in figure 2 with relative humidity equal to 0.6 at the lower boundary. Here the unsaturated region extends from the bottom to approximately $z = 0.45$ over which the relative humidity increases monotonically until the air is saturated, above which the solution has a shape similar to that in figure 1, with the fields and their first derivatives remaining continuous throughout.

5.3. *Stability of the drizzle solution*

In the absence of diffusion the stability of the drizzle solutions is related to the sign of the gradient of the linear function $m(z)$. Figure 3 gives the sign of this gradient

https://doi.org/10.1017/jfm.2018.954 Published online by Cambridge University Press

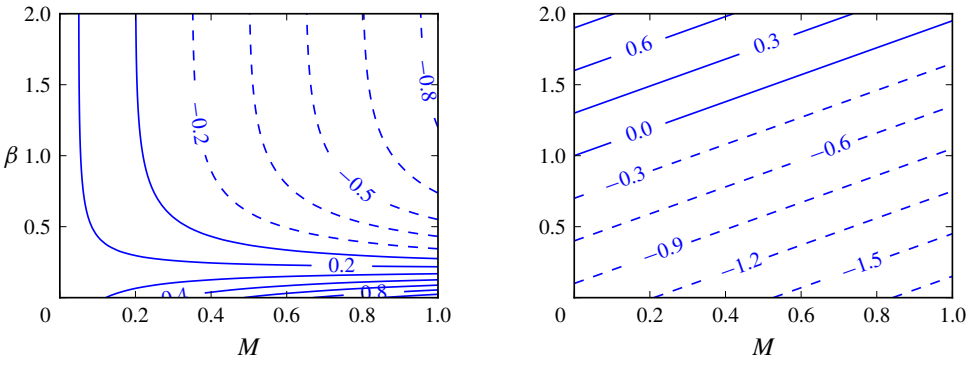


FIGURE 3. (Colour online) Contour plot of the value of the vertical gradient of $m(z) = b + \gamma q_s$ (i.e. $\partial m/\partial z$) in the drizzle solution as a function of β and γ, with $\alpha = 3$. Panel (a) imposes values of $b(0) = 0$ and $b(1) = 0.2$ with $T = b - \beta z$. Panel (b) has $T(0) = 0$ and $T(1) = -1$, with $b = T + \beta z$. The boundary values of q_s are calculated given the appropriate value of T. Convective instability is possible in the region of dashed lines.

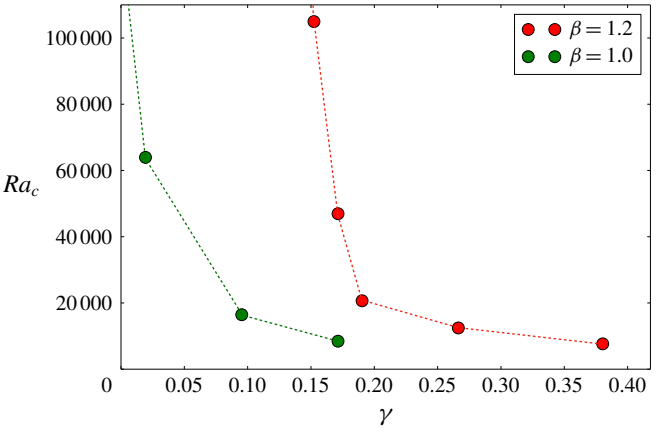


FIGURE 4. (Colour online) Stability of the linear drizzle solution. Graph of Ra_c versus γ for the drizzle solution at $\beta = 1$ (green) and $\beta = 1.2$ (red). The dots mark the numerically determined stability boundary, with instability occurring above and to the right of the dots.

as a function of the non-dimensional parameters γ and β for the problem with saturated boundaries. As expected when $\gamma = 0$ (and moisture plays no role) stability is guaranteed if $\beta > 1$ in the problem with specified temperature at the boundaries (right panel), and as γ is increased the critical β for non-diffusive stability increases linearly with γ.

In the presence of diffusion, the stability of the drizzle solution is determined by γ, β, Ra and α. Even for cases where instability is allowed in the non-diffusive case, instability in the diffusive cases only occurs for sufficiently high Ra. The critical Ra_c may be calculated by time-stepping from a slightly perturbed numerically calculated drizzle solution in a large domain followed by a bisection method. (The method thus strictly finds the stability with respect to small but not infinitesimal perturbations.) Figure 4 shows the critical Rayleigh number Ra_c as a function of γ for two different choices of β: $\beta = 1.0$ corresponds to a neutrally dry marginally stable atmosphere and

https://doi.org/10.1017/jfm.2018.954 Published online by Cambridge University Press

$\beta = 1.2$ corresponds to a stable dry atmosphere, for the case with saturated boundaries. We see that Ra_c approaches an asymptote at the non-diffusive threshold ($Ra \to \infty$), and as γ is increased the critical Rayleigh number decreases. For $\gamma = 0$ the problem is that of dry convection and the case with $\beta = 1.2$ is then always stable. The case with $\beta = 1.0$ and $\gamma = 0$ will be stabilized by any non-zero diffusivity, and is neutrally stable in the infinite Rayleigh-number limit.

6. Nonlinear results: initial value problems and statistical equilibration

In this section we discuss various results obtained with the full, time-dependent and nonlinear system. Specifically, we solve non-dimensional nonlinear equations (4.3)–(4.6), together with the physics equations (4.9), in two dimensions, with an aspect ratio of 20 and $Pr = S_m = 1$. In all experiments we set the atmosphere to be stable to dry convection, with $\beta = 1.2$, and set $\alpha = 3.0$. We first describe a sequence of experiments in which the Rayleigh number is varied, with all other parameters fixed, and then describe experiments with the parameter γ varying. The equations are solved numerically using the flexible spectral solver Dedalus. We use Fourier series in the horizontal, Chebyshev polynomials in the vertical, and third-order semi-implicit backward time differentiation. Heaviside functions are evaluated by $\mathcal{H}(\xi) \approx (1 + \tanh k\xi)/2$, with $k = 10^5$. Flows with positive and negative vertical velocity are referred to as upflows and downflows, respectively, with the words updraughts and downdraughts reserved for more coherent structures.

6.1. *Variation with the Rayleigh number*

In these experiments we vary the Rayleigh number but keep γ fixed, at $\gamma = 0.19$. These parameters give the possibility of continued instability of the drizzle solution to moist convection for sufficiently high Rayleigh numbers, as can be seen from figures 3 and 4(*b*). The initial conditions are typically chosen so that $q = 0$ in the interior of the domains except for a parcel of saturated air initially placed near the bottom boundary. This parcel immediately leads to heating and changes in the buoyancy field locally and triggers the start of moist convection. This initial condition naturally gives rise to plume triggering in the quiescent region of the domain before a statistically steady state is achieved, with the subsequent evolution depending on the Rayleigh number.

6.1.1. *Time dependence and basic properties*

For small enough Rayleigh numbers (e.g. $Ra = 10^2$) the action of diffusion damps out all motions and the system relaxes back to the drizzle solution, with saturation occurring everywhere in the domain. For high enough Ra the drizzle solution is unstable to small perturbations and the trigger leads to sustained convection. Figure 5 gives time series of the kinetic energy for increasing Ra, and figures 6 and 7 show the corresponding buoyancy and relative humidity evolution with time at $z = 0.5$ and using Hovmöller plots (i.e. space–time plots showing a time series). For the three smallest values of Ra the solution reaches a steady state and the kinetic energy approaches a constant value, which increases with Ra. For the three higher values of the Ra, the solution is unsteady and spatio-temporally modulated and as expected the average kinetic energy increases with Ra. Irregular time dependence of solutions appears to arise more easily in moist convection than in dry convection, at least in two dimensions, because of the sharp nature of the nonlinearities expressed by the thresholds in moist convection.

https://doi.org/10.1017/jfm.2018.954 Published online by Cambridge University Press

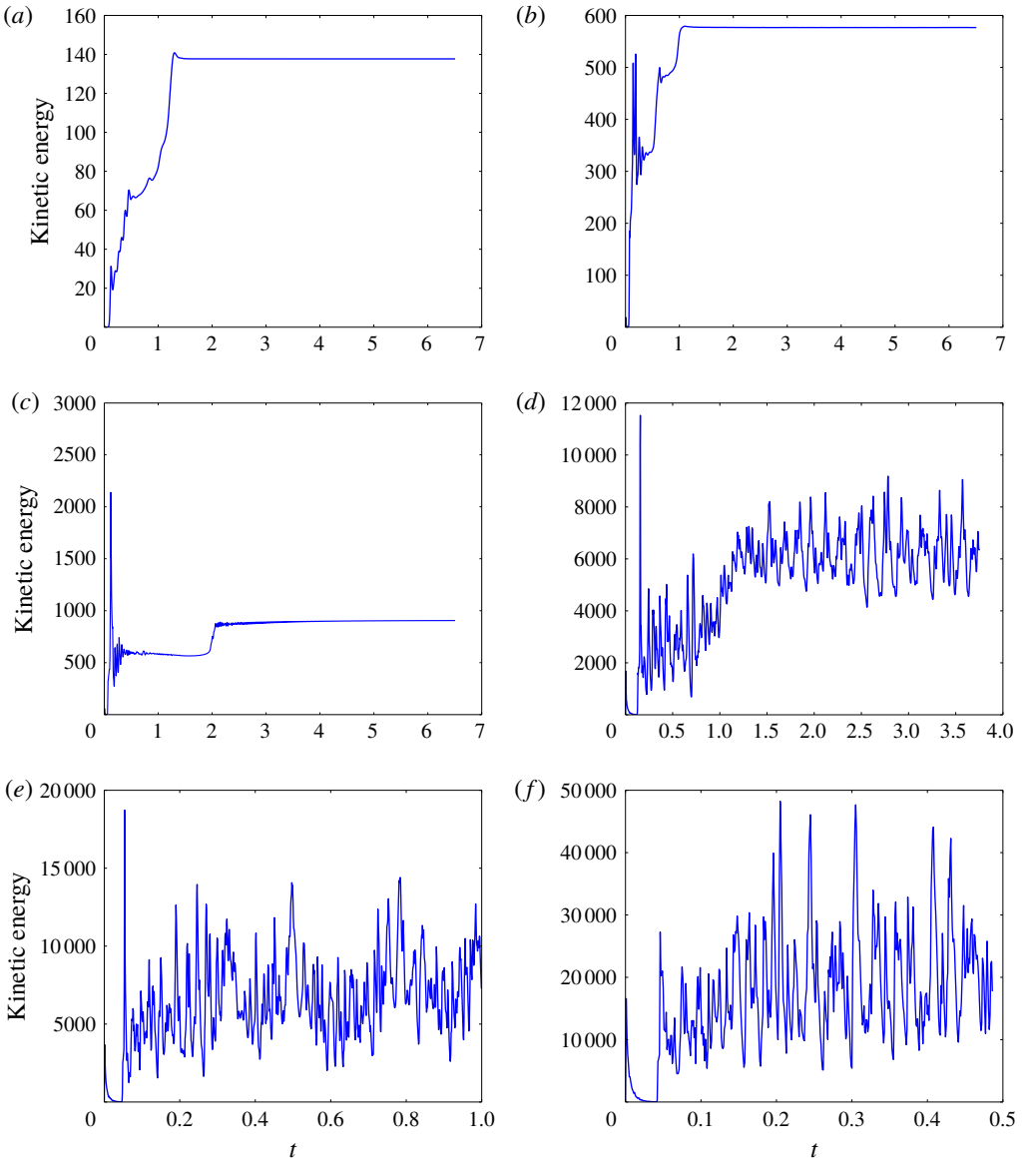


FIGURE 5. (Colour online) Time series for non-dimensional kinetic energy for numerical simulations with $\gamma = 0.19$ and (*a*) $Ra = 2 \times 10^5$, (*b*) $Ra = 1 \times 10^6$, (*c*) $Ra = 2 \times 10^6$, (*d*) $Ra = 2 \times 10^7$, (*e*) $Ra = 5 \times 10^7$, (*f*) $Ra = 2.5 \times 10^8$. The horizontal axis is time in diffusive units of H^2/κ, and note the differing scales of the axes in the panels.

The nature of time dependence in the solutions can be seen in some of the movies that are included in the supplementary material available online at https://doi.org/10.1017/jfm.2018.954. Movie 1 shows the evolution from the initial conditions for the four variables, b, q, T and u, for $Ra = 2 \times 10^5$. Initially the moist blob is seen in the q field and rapidly heats the parcel causing a deficit in the buoyancy field that leads to its rise. This buoyant rise triggers gravity waves that advect the

https://doi.org/10.1017/jfm.2018.954 Published online by Cambridge University Press

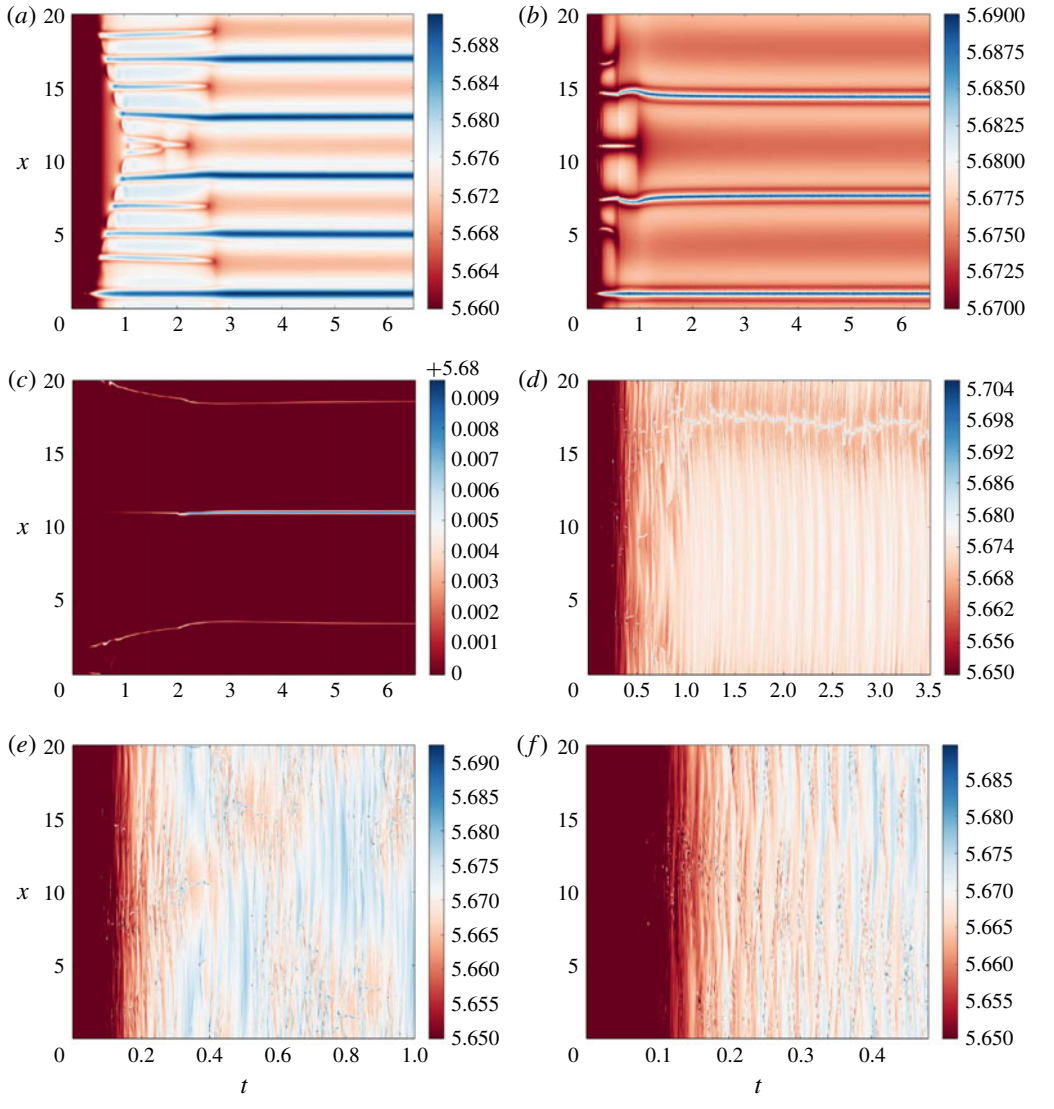


FIGURE 6. (Colour online) As for figure 5 but now time series (Hovmöller plots) at $z = 0.5$ and for all x for buoyancy for $\gamma = 0.19$ at (*a*) $Ra = 2 \times 10^5$, (*b*) $Ra = 1 \times 10^6$, (*c*) $Ra = 2 \times 10^6$, (*d*) $Ra = 2 \times 10^7$, (*e*) $Ra = 5 \times 10^7$, (*f*) $Ra = 2.5 \times 10^8$.

moisture field and thus triggers further buoyant patches to rise in the vicinity of the initial plume. This process continues until several (of the order of ten) buoyant plumes are found in the box. These plumes continue their evolution by sometimes merging and sometimes dying, until a steady state is reached with five equally spaced plumes in the box. The evolution is illustrated by Hovmöller plot of the buoyancy b as a function of x and t for fixed $z = 0.5$, shown in figure 6(*a*). The diagram clearly shows the triggering of plumes at the beginning of the calculation followed by their merging and approach to a steady state. Figure 6(*b*,*c*) shows that the dynamics is similar for the next two smallest values of Ra, but for $Ra = 2 \times 10^6$ there are only

https://doi.org/10.1017/jfm.2018.954 Published online by Cambridge University Press

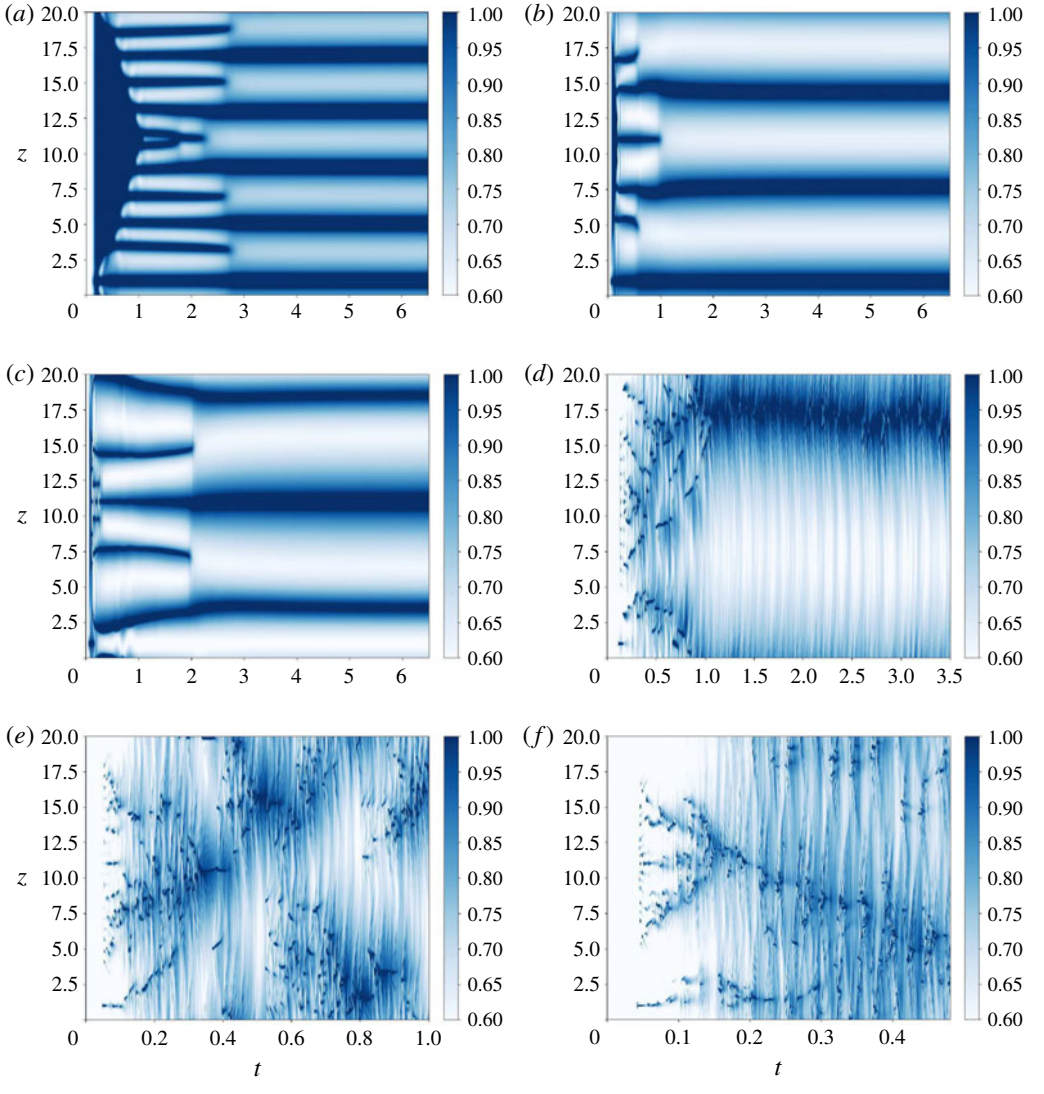


FIGURE 7. (Colour online) Time series (Hovmöller plots) for relative humidity (q/q_s) at $z = 0.5$ and for all x for $\gamma = 0.19$ at (*a*) $Ra = 2 \times 10^5$, (*b*) $Ra = 1 \times 10^6$, (*c*) $Ra = 2 \times 10^6$, (*d*) $Ra = 2 \times 10^7$, (*e*) $Ra = 5 \times 10^7$, (*f*) $Ra = 2.5 \times 10^8$.

three plumes in the computational domain at the end of the calculation, with a wider spacing between plumes.

Movies 2–4 show the evolution for $Ra = 2 \times 10^7$, 5×10^7 and 2.5×10^8 respectively. They show that the buoyant parcel rapidly triggers turbulent moist convection for these Rayleigh numbers. Here the plumes are much more time-dependent and for $Ra = 2 \times 10^7$ eventually the system is left in a state with a single, extremely time-dependent plume in the computational domain. This plume is very efficient at driving gravity waves, though for these parameters the waves are not instrumental in triggering plumes at other locations in the computational domain (as shown in figure 6*d*). However as the Rayleigh number is increased multiple plumes are found

https://doi.org/10.1017/jfm.2018.954 Published online by Cambridge University Press

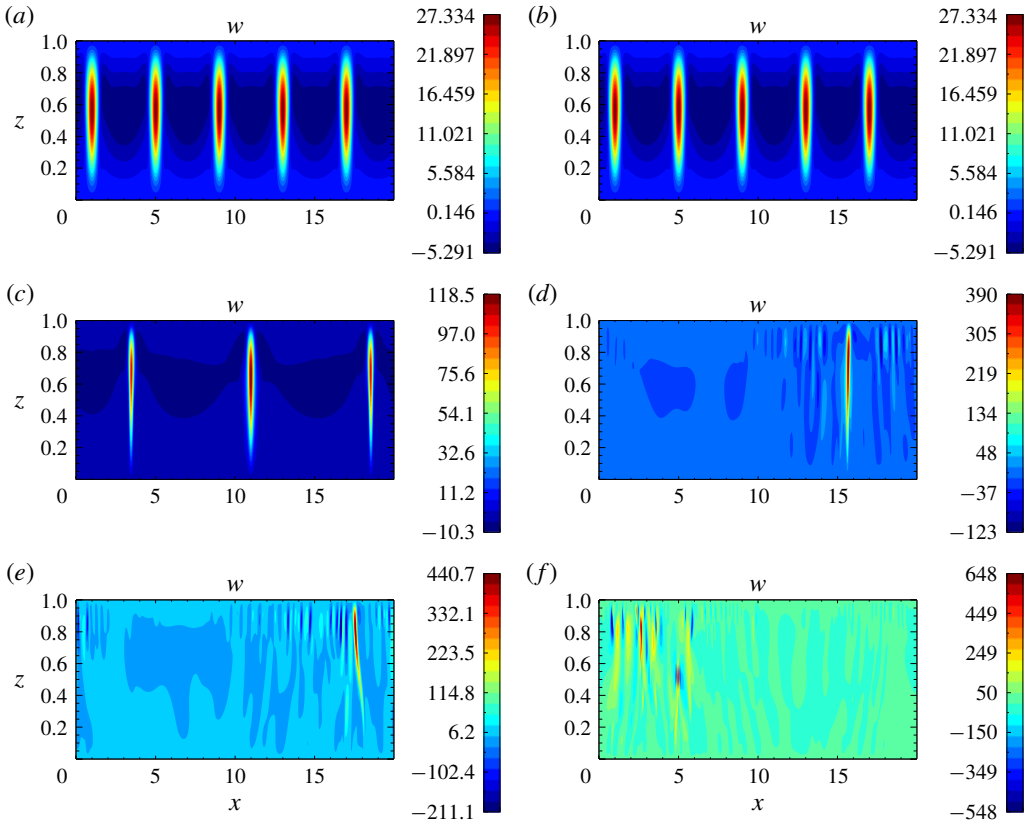


FIGURE 8. (Colour online) Snapshots of vertical velocity in a statistically equilibrated state for $\gamma = 0.19$ at (*a*) $Ra = 2 \times 10^5$, (*b*) $Ra = 1 \times 10^6$, (*c*) $Ra = 2 \times 10^6$, (*d*) $Ra = 2 \times 10^7$, (*e*) $Ra = 5 \times 10^7$, (*f*) $Ra = 2.5 \times 10^8$.

in the domains, triggered by the gravity waves. These plumes are born and die rapidly as shown in the Hovmöller plots of figure 6(*e*,*f*). The triggering by the gravity waves for the turbulent solutions is most clearly seen in figure 7(*d*–*f*).

Figures 8 and 9 show snapshots of the spatial dependence of the solutions in a statistically equilibrated state for the vertical velocity (w) and the relative humidity (defined as $q/q_s(T)$). For the steady solutions the solution takes the form of strong narrow updraughts surrounded by broader gentler downdraughts. The asymmetry is a well-known result in moist atmospheric convection (e.g. Ludlam 1980), but in Boussinesq Rayleigh–Bénard convection the updraughts and downdraughts have exactly the same properties because of the up–down symmetry in the problem.

As the Rayleigh number is increased the updraughts become thinner and sparser and at high enough Rayleigh numbers they become unstable. For these higher Rayleigh numbers the plumes are extremely thin (and as noted earlier, very time-dependent). The relative humidity shows that for a moderate Rayleigh number the flow is saturated (red colour) in the updraughts and in the diffusive layers at the top and bottom of the computational domain. The downdraughts are in general not saturated since they are bringing dry air down into regions with higher temperatures where q_s is larger, and the horizontally averaged relative humidity is a minimum in the domain interior, as discussed more below.

https://doi.org/10.1017/jfm.2018.954 Published online by Cambridge University Press

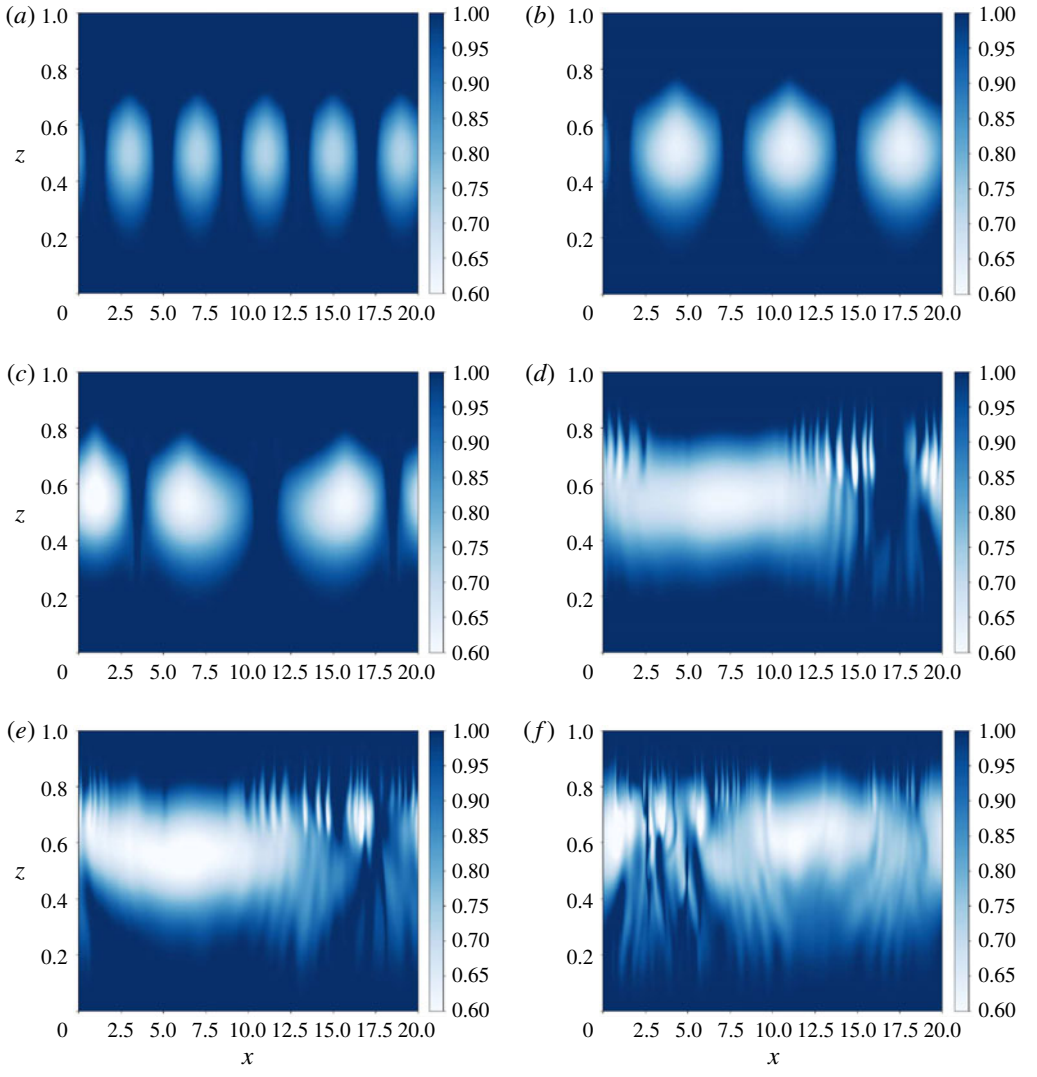


FIGURE 9. (Colour online) Snapshots of relative humidity in a statistically equilibrated state for $\gamma = 0.19$ at (*a*) $Ra = 2 \times 10^5$, (*b*) $Ra = 1 \times 10^6$, (*c*) $Ra = 2 \times 10^6$, (*d*) $Ra = 2 \times 10^7$, (*e*) $Ra = 5 \times 10^7$, (*f*) $Ra = 2.5 \times 10^8$.

6.1.2. *Equilibrated properties*

Equilibration of the moist convective solution is more complicated than in the dry problem. Roughly speaking, dry Rayleigh–Bénard convection equilibrates by mixing the buoyancy to an adiabatic profile in the core, thus effectively removing the driving except in thermal boundary layers at the top and bottom of the domain leaving the neutral profile, $\partial b/\partial z \approx 0$, in the interior. In moist convection the analogous solution is a state corresponding to the saturated adiabatic lapse rate. In atmospheric models that cannot resolve convection, a simple convective parametrization is to adjust the buoyancy profile to satisfy these criteria, although adjustment methods are now commonly regarded as over-simple because the implied separation of time scales

https://doi.org/10.1017/jfm.2018.954 Published online by Cambridge University Press

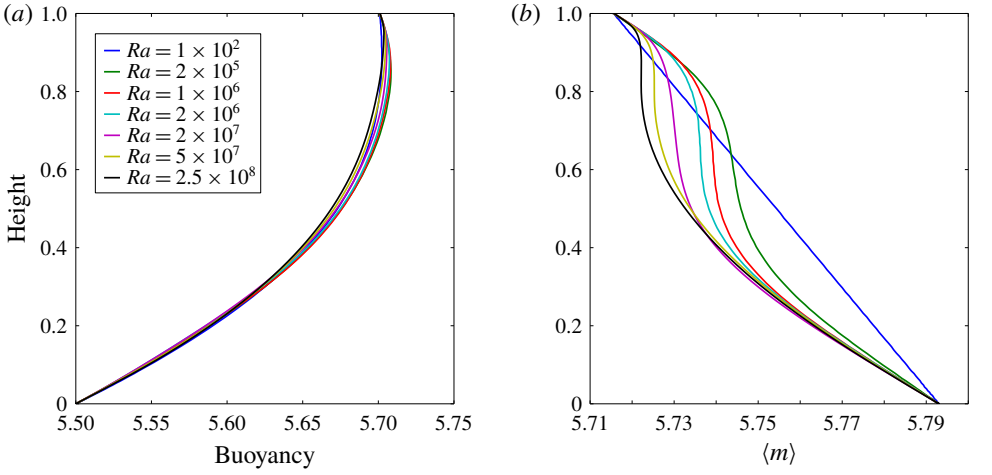


FIGURE 10. (Colour online) Horizontally averaged profiles for (*a*) buoyancy and (*b*) $m(z)$ for $\gamma = 0.19$ and a range of Ra.

is too extreme (although improved parametrizations are hard to come by). To get a sense of the equilibration processes here we will show how various profiles vary as a function of Rayleigh number, with detailed analysis left for future work.

Figure 10 shows the horizontally averaged profiles in the statistically equilibrated state for the buoyancy and m. Both are significantly modified by convection – recall that m has a linear profile in z in the saturated drizzle solution, which is reproduced only by the $Ra = 1 \times 10^2$ solution. The corresponding profiles in the upflows and downflows alone are shown in figure 11. These profiles show fairly uniform values of m in the upper part of the domain, but the degree to which this is caused by mixing and/or adjustment through gravity waves in subsiding regions will be investigated in a subsequent paper. The lower part of the domain remains unstable even at high Rayleigh number (see also figure 18*c*), and whether this result holds at still higher Rayleigh number, and in three dimensions, is also a topic for future investigation. The buoyancy fluxes giving rise to these profiles are shown in figures 12 and 13. In both the steady and unsteady cases the buoyancy flux is peaked in the upper half of the domain, in fact close to the diffusive upper boundary layer in the unsteady case. The moisture flux (not shown) peaks lower down, largely because there is much more moisture where the temperature is higher.

Figure 14 shows the kinetic energy and the fraction of the domain covered by near-saturated upflows as a function of Ra. As expected (at least for moderate values of Rayleigh number, and given that the Reynolds number is often taken to be the square root of the Rayleigh number) the kinetic energy increases with Ra. The area fraction of upflows has a more complicated dependence, and depends on the criterion used. For the steady solutions (the lowest three values of Ra) the area fraction actually decreases with Ra if the weakest criterion ($w > 0$) is used. As Ra is increased further the solutions become time-dependent and the area fraction of upflows stays roughly constant – the strong upflows are very narrow, but there are a greater number of weak upflows. However, this criterion is most likely picking up flows with positive vertical velocity due to gravity waves and not associated with updraughts, and this V-shaped dependence is in fact reproduced without any restriction

https://doi.org/10.1017/jfm.2018.954 Published online by Cambridge University Press

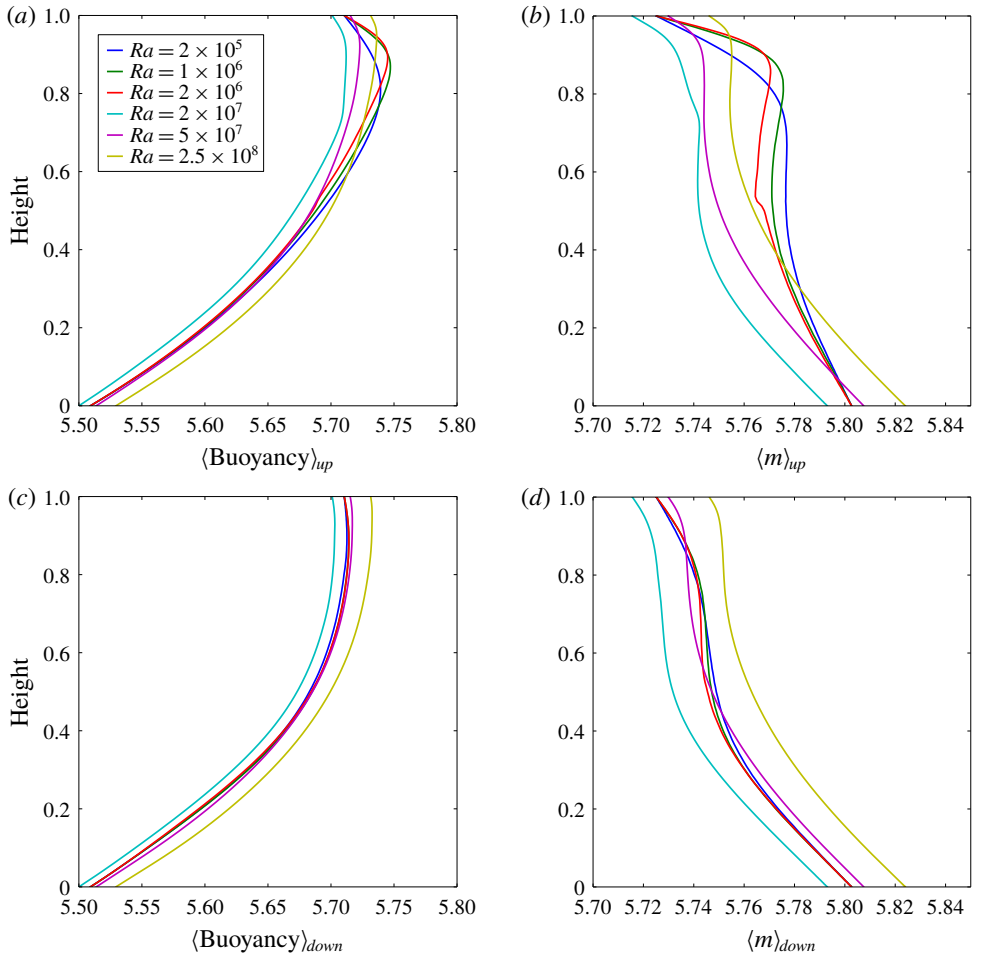


FIGURE 11. (Colour online) (*a*,*b*) Averages taken over the upflows alone (where $w > 0$) of (*a*) the buoyancy and (*b*) the moist static energy, m. (*c*,*d*) The same, except that averages are taken over downflows alone (where $w < 0$).

on relative humidity. With the more restrictive criteria (red and green lines in the figure) the upflow fraction decreases and then seems to converge to a definite value as Rayleigh number increases, with the structures generally remaining space filling. Understanding the parameter dependence of these results, and whether there is any universality, is of direct relevance to meteorology, since 'mass flux parametrization schemes' commonly used in coarse resolution atmospheric models often assume that updraughts occupy some fixed fraction of the domain.

6.1.3. *Relative humidity*

Relative humidity has no analogue whatsoever in the dry system but is of fundamental importance to the climate system. In the fast condensation limit, and at high Reynolds number, the relative humidity of a parcel is largely determined by the temperature of the location at which it was last saturated, since in the absence of condensation or re-evaporation (which in some situations is quite important) a parcel

https://doi.org/10.1017/jfm.2018.954 Published online by Cambridge University Press

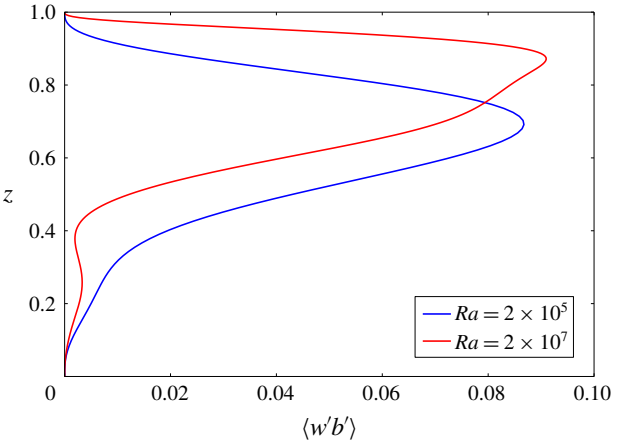


FIGURE 12. (Colour online) Time and horizontally averaged vertical buoyancy flux, $\langle w'b' \rangle$, at two values of Rayleigh number. Note the peak flux rising up to the top boundary layer at higher Rayleigh number. The time series of these fields are shown in figure 13.

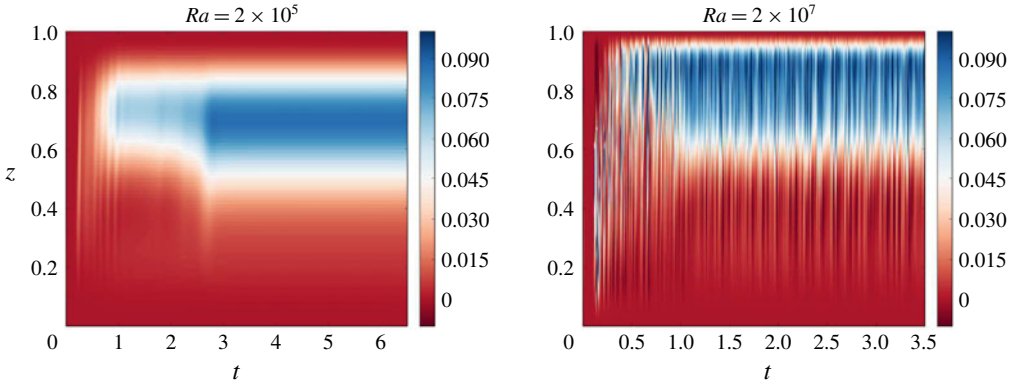


FIGURE 13. (Colour online) Time series (Hovmöller plots) of the x-averaged buoyancy fluxes $\langle w'b' \rangle$ at each height, at two values of Rayleigh number. The time-averaged fields, over the later parts of the time period, are shown in figure 12.

conserves its specific humidity. Thus, updraughts tend to be saturated (the parcels are moving to lower temperatures) and downdraughts unsaturated, but quantitatively determining the vertical profile is non-trivial, especially as the flow becomes turbulent and the updraughts entrain dryer air from the surroundings.

In our system, there is a relative humidity minimum at mid-levels and the values in the minimum decrease, albeit slowly, as Rayleigh number is increased (figure 15). Such a minimum is also seen in atmospheric observations in convecting regions and is discussed by Romps (2014). This asymmetric C-shaped profile arises in our simulations for two reasons. The first is that the fraction of the domain covered by upflows decreases as the Rayleigh number increases (figure 14). For the laminar flows the upflows remain saturated so that a decrease in their volume fraction is significant. For the unsteady cases the average relative humidity of the upflows tends to decrease with Rayleigh number, a signature of the turbulent vertical upflows

https://doi.org/10.1017/jfm.2018.954 Published online by Cambridge University Press

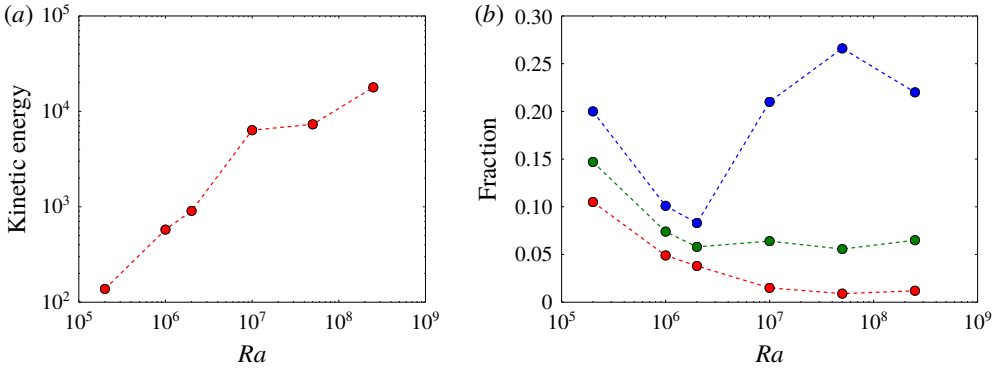


FIGURE 14. (Colour online) (*a*) Kinetic energy as a function of *Ra*. (*b*) Area fraction of near-saturated upflows as a function of *Ra*, with three different criteria. The blue line requires $w > 0$ and $RH > 0.95$, the green line requires $w > 0.02w_{max}$ and $RH > 0.95$ and the red line requires $w > 0.1w_{max}$ and $RH > 0.95$.

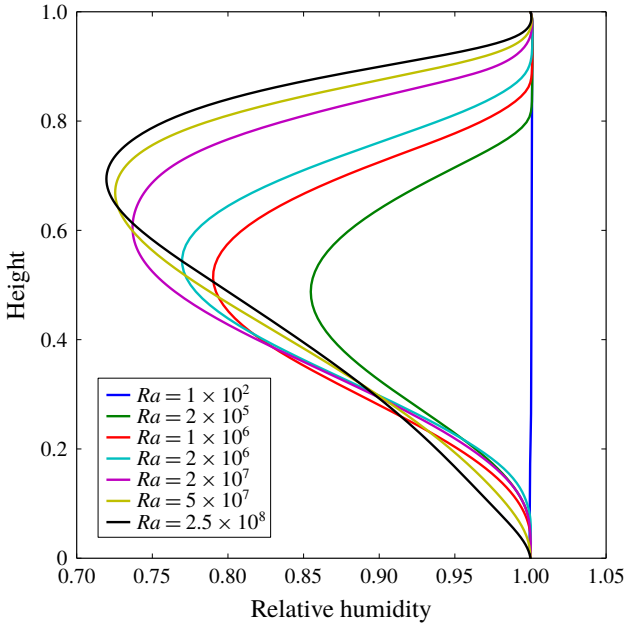


FIGURE 15. (Colour online) Horizontally averaged relative humidity over a range of Rayleigh numbers, with all other parameters fixed.

entraining relatively dry material into their flanks from the ambient background, even as the core remains saturated. This entrainment of relatively dry air also contributes to the decrease of m in the upflows. The second factor is more specific to this model – as the Rayleigh number increases, the turbulent convection mixes moisture more effectively and the boundary layer at the top of the domain where the atmosphere is forced to return to a saturated state by the top boundary conditions becomes thinner. However, numerical simulations with an upper boundary condition of no moisture flux (i.e. $\partial q/\partial z = 0$ at $z = 1$) in fact show similar behaviour, in particular having a

https://doi.org/10.1017/jfm.2018.954 Published online by Cambridge University Press

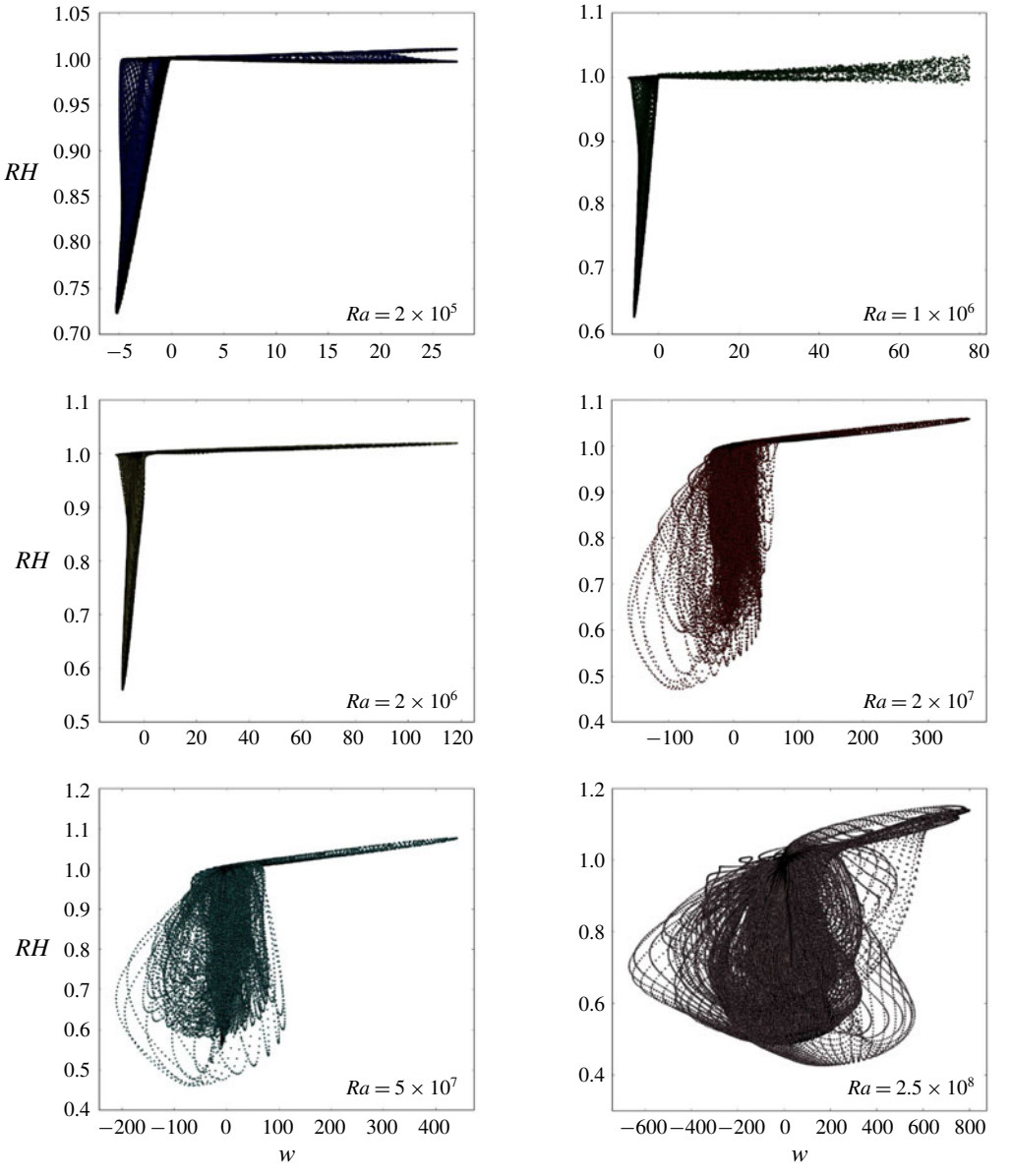


FIGURE 16. (Colour online) Scatter plots of relative humidity, *RH*, and vertical velocity, *w*, over a range of Rayleigh numbers, as labelled. Note the changes in the scale of the *x*-axis.

similar C-shaped relative humidity profile with minimum in the domain interior (not shown), so this effect may be less important.

Variations in the relative humidity distribution may be graphically illustrated with a series of scatter plots of *w* and *RH* at various values of *Ra* (figure 16). At the lower values of *Ra* the distributions exhibit two narrow limbs: the strongly ascending air is close to saturated (top, near-horizontal limb), while the air that is significantly sub-saturated is all weakly subsiding (left, near-vertical limb). In this regime, as *Ra*

https://doi.org/10.1017/jfm.2018.954 Published online by Cambridge University Press

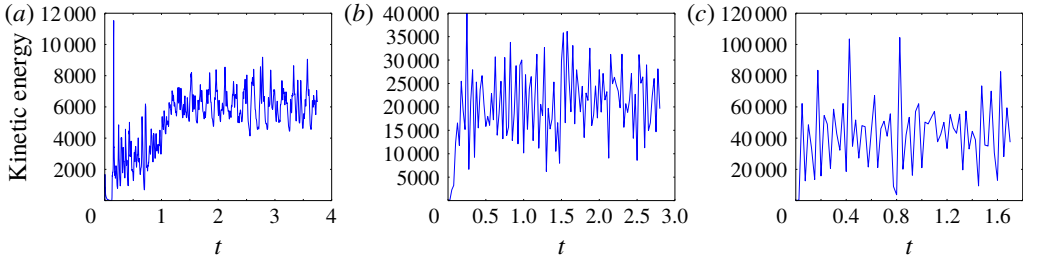


FIGURE 17. (Colour online) Time series for kinetic energy at $Ra = 2 \times 10^6$ for (*a*) $\gamma = 0.19$, (*b*) $\gamma = 0.38$ and (*c*) $\gamma = 0.76$. Note the different scales on the vertical axes.

increases from $Ra = 2 \times 10^5$ to $Ra = 2 \times 10^6$, the updraughts get stronger and the regions of subsidence get drier. At $Ra = 2 \times 10^7$ the distribution of w and RH changes significantly with the onset of unsteadiness leads to the generation of gravity waves in the domain (cf. figure 5*d*). In the subsaturated limb there are now wide distributions of w, representing both mean subsidence and regions of local ascent, both with broad relative humidity distributions. In this unsaturated part of the domain RH increases with upward parcel displacement and thus for a gravity-wave-like solution – where w and displacement are out of phase – the solution forms closed loops. As Ra increases further, in figure 16(*d–f*), the solutions become increasingly turbulent and the maximum w and minimum RH in the two limbs of the distribution become more extreme (note the scales of the axes are changing). Interestingly, for the very highest Ra there are points on the margins of the cloudy updraughts that appear to transition smoothly from conditions of vigorous, saturated ascent (high w and $RH \approx 1$) to the ambient conditions of lower RH and w. In this regime, the cloudy updraughts are becoming diffused, so that they are carrying subsaturated air on their flanks, a feature that is not seen at the lower values of Ra. The updraughts in this turbulent regime are entraining dryer, unsaturated air into their margins, giving rise to a broader distribution of relative humidity in their unsteady flanks, but the presence of gravity waves is still seen in the distinctive patterns of the scatter plots.

6.2. *Variation with condensational parameter, γ*

We now focus on the role of the (non-dimensional) condensation parameter γ, with other parameters fixed. As discussed earlier, changing γ modifies the stability of the drizzle solution (as shown in figure 3). For fixed $\beta > 1$ and small γ the drizzle solution will remain stable whatever the value of Ra. As γ is increased the gradient of $m(z)$ is altered until it becomes negative and instability occurs if the Rayleigh number is sufficiently high. We thus conduct a series of experiments for moderately high Ra ($Ra = 2 \times 10^6$) and with all other parameters as before, and vary γ. For $\gamma \lesssim 0.13$ the drizzle solution is linearly stable for all Ra. Numerical solutions in fact indicate that for $\gamma \lesssim 0.13$ the solution always returns to the drizzle solution. As γ is increased further, steady then unsteady nonlinear solutions are found, and time series of the kinetic energy for $\gamma = 0.19$, 0.38 and 0.76 are shown in figure 17. As expected, as γ is increased the kinetic energy of solutions increases, appearing to scale roughly linearly with γ for large γ.

Figure 18 shows the effect of varying γ on the mean profiles of buoyancy, relative humidity and m. As the heating is increased (by increasing γ) the buoyancy of the

https://doi.org/10.1017/jfm.2018.954 Published online by Cambridge University Press

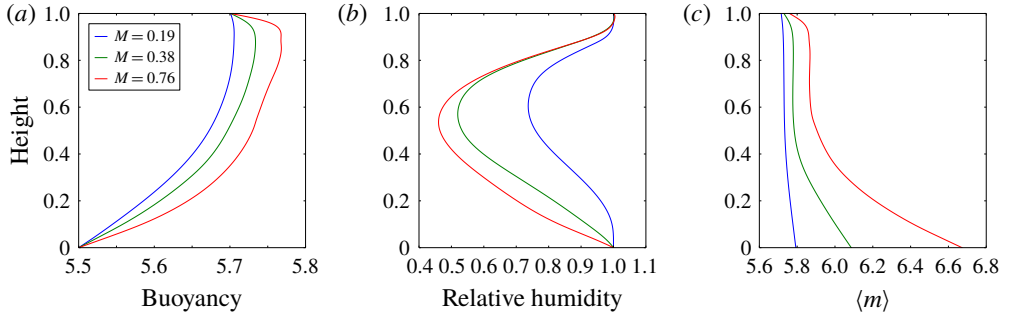


FIGURE 18. (Colour online) Horizontally averaged profiles for (*a*) buoyancy, (*b*) relative humidity and (*c*) $m(z)$ for $Ra = 2 \times 10^6$ and a range of γ. Note the different horizontal scale for $\langle m \rangle$ from those of earlier figures showing $\langle m \rangle$.

layer is increased and the relative humidity decreased. The net effect is to increase m, with m being well mixed between $z = 0.5$ and a thin boundary layer near to the top of the domain. The lower half of the domain remains convectively unstable (as noted earlier), and whether it becomes neutralized at higher values of the Rayleigh number is a topic for future investigation.

We conclude with a remark on subcritical convection – i.e. sustained convection occurring for $Ra < Ra_c$, where Ra_c is the critical Rayleigh number at which the linear instability of the drizzle solution occurs. No such behaviour has been found for this two-dimensional model for an aspect ratio of 20, suggesting global (nonlinear) stability for this configuration. On the other hand, Pauluis & Schumacher (2011) and Weidauer, Pauluis & Schumacher (2011) did appear to find occurrences of sustained convection in a regime they deemed subcritical by a different criterion and in a different system from ours. *Pace* their results, we are unable to say whether sustained subcritical convection is a general property of moist convection.

7. Discussion and conclusions

In this paper we have presented and begun to analyse a simple model system for moist convection. The literature on moist convection is large but has little overlap with the even larger literature on Rayleigh–Bénard convection, with a few exceptions as noted in the introduction. Our goals are both to make that connection stronger and to explore moist convection at a fundamental level. To these ends, we precisely define a relatively simple moist system and look at how that system behaves as the governing non-dimensional parameters change, passing from a stationary diffusive-condensing state to a turbulent, time-dependent state.

The system itself, defined by (2.25), comprises the ideal-gas Boussinesq equations plus an evolution equation for humidity q, a definition of temperature and saturation humidity, and a simple recipe for condensation and its effect on buoyancy. The key non-dimensional parameters may be readily identified: in addition to the familiar Rayleigh and Prandtl numbers, the effects of moisture are captured by the parameter γ, as in (4.7), or alternatively a 'condensational Rayleigh number', R_γ, defined in (4.11). Other non-dimensional numbers arise from the simplified Clausius–Clapeyron relation and the relation between temperature and buoyancy. The model system thus simply captures the essential difference between moist and dry convection, reducing

https://doi.org/10.1017/jfm.2018.954 Published online by Cambridge University Press

to the conventional dry Rayleigh–Bénard system as the single parameter γ goes to zero.

The model possesses a drizzle solution of no motion, given by a linear profile of moist static energy $m(z)$. If the boundaries are saturated then so is the interior, and an exact solution may be obtained in which the diffusion of moisture is balanced by condensation, with the condensation providing a source in the buoyancy equation that is also balanced by diffusion. This balance determines the temperature, and so the saturation value of humidity and so the condensation. The problem is thus inherently nonlinear, although a wholly analytic solution may be written down in terms of a special function. A drizzle solution may also be found if the lower boundary is not saturated, in which case saturation occurs above some height inside the domain, as in figure 2. The drizzle solution is unstable if the Rayleigh number is high enough and if the values γ and the boundary conditions are such that the gradient of $m(z)$ is negative, and a numerically obtained stability boundary is shown in figure 4. For values of parameters that are linearly unstable we always find a solution with motion, and for values of parameters that are linearly stable we always find convergence to the stationary drizzle solution, albeit sometimes after extended transient periods with time-dependent flow. However, we ascribe no generality to this result.

Numerical solutions of the full system show that, as the Rayleigh number increases, the solution transitions from the steady drizzle solution to a state with a small number of time invariant plumes, and then to a time-dependent and ultimately a turbulent state, with plumes generating gravity waves that remotely trigger other plumes and so on. Typically, solutions are less steady than corresponding solutions at similar Rayleigh numbers in the dry problem, with the plume separation determined by the drying effects of downwelling between the plumes. The plumes are completely saturated when laminar, but entrain dry air into their flanks when unsteady, more so as the Rayleigh number further increases into a more turbulent regime, with the associated gravity waves giving rise to distinctive patterns of relative humidity (figure 16). Overall, the domain becomes dryer in the interior as the system becomes more unstable, although the simulations may be suggesting that the vertical structure of the relative humidity is tending to a well-defined limit (figure 15). Clearly, it would be of interest to examine all these issues in three dimensions and at higher Rayleigh number, with the simplicity of the system suggesting that the parameter dependence of the solutions, including such things as the plume width and separation, could, in principle, be unambiguously determined.

The parameter dependence of the moist system at very high Ra is of particular interest. In the dry problem, and with smooth upper and lower boundaries, theoretical, numerical and laboratory studies all suggest that the solutions always depend upon Rayleigh number; that is, there is no Rayleigh-number-independent ultimate regime. It seems unlikely that the presence of moisture alone will alter this conclusion, since the moisture must still enter the domain diffusively through the lower boundary. It is, however, widely believed that the properties of convection in Earth's atmosphere do not, in fact, depend on the molecular diffusivity and viscosity, and properly understanding this issue remains a significant challenge. We might conjecture that radiative forcing, which provides a source of buoyancy independent of diffusivity, could remove the dependence of atmospheric convection on molecular diffusion and viscosity. Other possibilities exist, such as a rough boundary and turbulence in the boundary layer generated independently of convection, as suggested by success of the Monin–Obukhov theory, which has no explicit dependence on molecular properties but which does rely on a roughness length.

https://doi.org/10.1017/jfm.2018.954 Published online by Cambridge University Press

Many other studies need to be performed with the model presented here to better understand it. A well-defined pathway toward more realism may also be defined: using an anelastic model instead of a Boussinesq one, adding liquid water and re-evaporation, removing the effects of the upper boundary, and/or adding radiation all lead toward the more complex type of model commonly used in moist atmospheric convection, and we hope that other investigators will also pursue these and related problems. By ensuring that any more complex model is precisely defined and is connected in a direct fashion to a more simple model, one may hope that the results obtained are both reproducible and understandable.

Acknowledgements

Our simulations use the Dedalus framework (Burns *et al.* 2016 and http://dedalus-project.org). We thank the Dedalus team for their fine software and especially J. Oishi for his endless patience. We also thank J. Vanneste for drawing our attention to the Lambert W function, J. Sieber for conversations and pointing out an error in an earlier draft, and K. Emanuel and three anonymous reviewers for their comments. This work was funded by NERC under the Paracon Program via grants NE/N013123/1 and NE/N013840/1 to the Universities of Exeter and Leeds. G.K.V. and D.J.P. also acknowledge support through Royal Society Wolfson Research Merit Awards, and S.M.T. acknowledges support from the ERC.

Supplementary movies

Supplementary movies are available at https://doi.org/10.1017/jfm.2018.954.

Appendix A. Other non-dimensionalizations

A.1. *Buoyancy-based non-dimensionalization*

A buoyancy-based non-dimensionalization uses the buoyancy differences across the layer rather than diffusion to scale time, and hence velocity, and

$$t_s = \left(\frac{H\theta_0}{g\Delta T}\right)^{1/2}, \quad U = W = \left(\frac{g\Delta T H}{\theta_0}\right)^{1/2}. \tag{A 1a,b}$$

The other scales are the same as with the diffusive non-dimensionalization. The non-dimensional momentum equation is

$$\frac{\mathrm{D}\widehat{\boldsymbol{v}}}{\mathrm{D}\widehat{t}} = -\boldsymbol{\nabla}\widehat{\phi} + b\boldsymbol{k} + \left(\frac{Pr}{Ra}\right)^{1/2}\nabla^2\widehat{\boldsymbol{v}}, \tag{A 2}$$

and a Reynolds number, $Re \sim Ra^{1/2}$, now appears in the viscous term as expected. The non-dimensional buoyancy equation is

$$\frac{\mathrm{D}\widehat{b}}{\mathrm{D}t} = \widehat{\gamma}\frac{q - q_s}{\widehat{\tau}}\mathcal{H}(\widehat{q} - \widehat{q}_s) + \frac{1}{(RaPr)^{1/2}}\nabla^2\widehat{b}, \tag{A 3}$$

and the non-dimensional moisture equation is

$$\frac{\mathrm{D}\widehat{q}}{\mathrm{D}t} = \frac{\widehat{q}_s - \widehat{q}}{\widehat{\tau}}\mathcal{H}(\widehat{q} - \widehat{q}_s) + \frac{1}{(RaPr')^{1/2}}\nabla^2\widehat{q}, \tag{A 4}$$

where $Pr' = \nu/\kappa_q = PrS_m$. The physics equations are unaltered from the case with diffusive scaling.

https://doi.org/10.1017/jfm.2018.954 Published online by Cambridge University Press

A.2. *Moisture-based non-dimensionalization*

We now use buoyancy created by condensation as a scaling. Thus we choose

$$t_s = \left(\frac{H}{q_0\gamma}\right)^{1/2}, \quad U = W = (\gamma q_0 H)^{1/2}, \quad B = \gamma q_0, \quad \text{so that } b = \gamma q_0 \widehat{b}. \tag{A 5a–c}$$

The momentum equations become

$$\frac{\mathrm{D}\widehat{\boldsymbol{v}}}{\mathrm{D}t} = -\boldsymbol{\nabla}\widehat{\phi} + \widehat{b}\boldsymbol{k} + \frac{Pr}{R_\gamma^{1/2}}\nabla^2\widehat{\boldsymbol{v}}, \tag{A 6}$$

where R_γ, the condensational Rayleigh number, is given by

$$R_\gamma = \frac{\gamma q_0 H^3}{\kappa\nu} = \frac{gLH^3 q_0}{c_p\theta_0\kappa\nu}. \tag{A 7}$$

Related moist Rayleigh numbers also appear in the analyses of Bretherton (1988) and Pauluis & Schumacher (2011).

The non-dimensional buoyancy equation is

$$\frac{\mathrm{D}\widehat{b}}{\mathrm{D}\widehat{t}} = \frac{\widehat{q} - \widehat{q}_s}{\widehat{\tau}}\mathcal{H}(\widehat{q} - \widehat{q}_s) + \frac{1}{(R_\gamma Pr)^{1/2}}\nabla^2\widehat{b}, \tag{A 8a}$$

and the non-dimensional moisture equation is

$$\frac{\mathrm{D}\widehat{q}}{\mathrm{D}\widehat{t}} = \frac{\widehat{q}_s - \widehat{q}}{\widehat{\tau}}\mathcal{H}(\widehat{q} - \widehat{q}_s) + \frac{1}{(R_\gamma Pr')^{1/2}}\nabla^2\widehat{q}. \tag{A 8b}$$

Here $\widehat{\tau}$ is the condensation time measured in units of the buoyancy time scale, and this is always a small number in the fast condensation limit. These equations have no parameter in the heating term in the buoyancy equation due to moisture condensation. However, the effect of the parameter has not been lost for it appears in boundary conditions. For example, if we require a dimensional drop of Δb across the domain we implement this with

$$\widehat{b}(\widehat{z} = 0) = 0, \quad \widehat{b}(\widehat{z} = 1) = \frac{\Delta b}{q_0\gamma} = \frac{\Delta b c_p\theta_0}{gLq_0}. \tag{A 9a,b}$$

REFERENCES

AHLERS, G., GROSSMANN, S. & LOHSE, D. 2009 Heat transfer and large scale dynamics in turbulent Rayleigh–Bénard convection. *Rev. Mod. Phys.* **81** (2), 503–537.

AMBAUM, M. H. P. 2010 *Thermal Physics of the Atmosphere*. Wiley.

AMERICAN METEOROLOGICAL SOCIETY 2018 Glossary of meteorology. Available online at http://glossary.ametsoc.org/wiki/.

BERLENGIERO, M., EMANUEL, K. A., VON HARDENBERG, J., PROVENZALE, A. & SPIEGEL, E. A. 2012 Internally cooled convection: a fillip for Philip. *Comm. Nonlin. Sci. Num. Sim.* **17** (5), 1998–2007.

https://doi.org/10.1017/jfm.2018.954 Published online by Cambridge University Press

BRETHERTON, C. S. 1987 A theory for nonprecipitating moist convection between two parallel plates. Part I. Thermodynamics and 'linear' solutions. *J. Atmos. Sci.* **44** (14), 1809–1827.

BRETHERTON, C. S. 1988 A theory for nonprecipitating convection between two parallel plates. Part II. Nonlinear theory and cloud field organization. *J. Atmos. Sci.* **45** (17), 2391–2415.

BRUN, A. S. & BROWNING, M. K. 2017 Magnetism, dynamo action and the solar–stellar connection. *Living Rev. Solar Phys.* **14**, 4.

BRYAN, G. H., WYNGAARD, J. C. & FRITSCH, J. M. 2003 Resolution requirements for the simulation of deep moist convection. *Mon. Wea. Rev.* **131** (10), 2394–2416.

BURNS, K. J., VASIL, G. M., OISHI, J. S., LECOANET, D. & BROWN, B. 2016 Dedalus: flexible framework for spectrally solving differential equations. Astrophysics Source Code Library: http://ascl.net/1603.015.

CHANDRASEKHAR, S. 1961 *Hydrodynamic and Hydromagnetic Stability*. Oxford University Press; reprinted by Dover Publications, 1981.

CHILLÀ, F. & SCHUMACHER, J. 2012 New perspectives in turbulent Rayleigh–Bénard convection. *Eur. Phys. J.* E **35** (7), 58.

CHRISTENSEN, U. 1995 Effects of phase transitions on mantle convection. *Annu. Rev. Earth Planet. Sci.* **23** (1), 65–87.

CROSS, M. C. & HOHENBERG, P. C. 1993 Pattern formation outside of equilibrium. *Rev. Mod. Phys.* **65** (3), 851.

DRAZIN, P. G. & REID, W. H. 1981 *Hydrodynamic Stability*. Cambridge University Press.

EMANUEL, K. A. 1994 *Atmospheric Convection*. Oxford University Press.

EMANUEL, K. A., NEELIN, J. D. & BRETHERTON, C. S. 1994 On large-scale circulations in convecting atmospheres. *Q. J. R. Meteor. Soc.* **120**, 1111–1143.

FRIERSON, D. M. W., HELD, I. M. & ZURITA-GOTOR, P. 2006 A gray radiation aquaplanet moist GCM. Part 1. Static stability and eddy scales. *J. Atmos. Sci.* **63**, 2548–2566.

GOLUBITSKY, M., SWIFT, J. W. & KNOBLOCH, E. 1984 Symmetries and pattern selection in Rayleigh–Bénard convection. *Physica* D **10** (3), 249–276.

GROSSMANN, S. & LOHSE, D. 2000 Scaling in thermal convection: a unifying theory. *J. Fluid Mech.* **407**, 27–56.

HERNANDEZ-DUENAS, G., MAJDA, A. J., SMITH, L. M. & STECHMANN, S. N. 2013 Minimal models for precipitating turbulent convection. *J. Fluid Mech.* **717**, 576–611.

KHAIN, A. P., BEHENG, K. D., HEYMSFIELD, A., KOROLEV, A., KRICHAK, S. O., LEVIN, Z., PINSKY, M., PHILLIPS, V., PRABHAKARAN, T., TELLER, A. *et al.* 2015 Representation of microphysical processes in cloud-resolving models: spectral (bin) microphysics versus bulk parameterization. *Rev. Geophys.* **53** (2), 247–322.

KRAICHNAN, R. H. 1962 Turbulent thermal convection at arbitrary Prandtl number. *Phys. Fluids* **5** (11), 1374–1389.

LAKKARAJU, R., STEVENS, R., ORESTA, P., VERZICCO, R., LOHSE, D. & PROSPERETTI, A. 2013 Heat transport in bubbling turbulent convection. *Proc. Natl Acad. Sci. USA* **110** (23), 9237–9242.

LOHSE, D. & TOSCHI, F. 2003 Ultimate state of thermal convection. *Phys. Rev. Lett.* **90** (3), 034502.

LUDLAM, F. H. 1966 Cumulus and cumulonimbus convection. *Tellus* **18**, 687–698.

LUDLAM, F. H. 1980 *Clouds and Storms: The Behavior and Effect of Water in the Atmosphere*. Penn. State University Press.

MAHRT, L. 1986 On the shallow motion approximations. *J. Atmos. Sci.* **43**, 1036–1044.

MARSHALL, J. C. & SCHOTT, F. 1999 Open-ocean convection: observations, theory, and models. *Rev. Geophys.* **37**, 1–64.

MELLOR, G. L. & YAMADA, T. 1974 A hierarchy of turbulence closure models for planetary boundary layers. *J. Atmos. Sci.* **31** (7), 1791–1806.

MITCHELL, J. L. & LORA, J. M. 2016 The climate of Titan. *Annu. Rev. Earth Planet. Sci.* **44**, 353–380.

MONIN, A. S. & OBUKHOV, A. M. 1954 Basic laws of turbulent mixing in the surface layer of the atmosphere. *Tr. Akad. Nauk SSSR Geophiz. Inst.* **24**, 163–187.

https://doi.org/10.1017/jfm.2018.954 Published online by Cambridge University Press

MORTON, B. R., TAYLOR, G. & TURNER, J. S. 1956 Turbulent gravitational convection from maintained and instantaneous sources. *Proc. R. Soc. Lond.* A **234**, 1–23.

O'GORMAN, P. A., ALLAN, R. P., BYRNE, M. P. & PREVIDI, M. 2012 Energetic constraints on precipitation under climate change. *Surv. Geophys.* **33** (3–4), 585–608.

O'GORMAN, P. A. & SCHNEIDER, T. 2006 Stochastic models for the kinematics of moisture transport and condensation in homogeneous turbulent flows. *J. Atmos. Sci.* **63**, 2992–3005.

PAPARELLA, F. & YOUNG, W. R. 2002 Horizontal convection is non-turbulent. *J. Fluid Mech.* **466**, 205–214.

PARODI, A., EMANUEL, K. A. & PROVENZALE, A. 2003 Plume patterns in radiative–convective flows. *New J. Phys.* **5** (1), 106.

PARSONS, B. & MCKENZIE, D. 1978 Mantle convection and the thermal structure of the plates. *J. Geo. Res.: Sol. Earth* **83** (B9), 4485–4496.

PAULUIS, O. & SCHUMACHER, J. 2010 Idealized moist Rayleigh–Bénard convection with piecewise linear equation of state. *Commun. Math. Sci.* **8** (1), 295–319.

PAULUIS, O. & SCHUMACHER, J. 2011 Self-aggregation of clouds in conditionally unstable moist convection. *Proc. Natl Acad. Sci. USA* **108** (31), 12623–12628.

PIERREHUMBERT, R. T., BROGNIEZ, H. & ROCA, R. 2007 On the relative humidity of the atmosphere. In *The Global Circulation of the Atmosphere: Phenomena, Theory, Challenges* (ed. T. Schneider & A. Sobel), pp. 143–185. Princeton University Press.

RAYLEIGH, LORD 1916 On convection currents in a horizontal layer of fluid, when the higher temperature is on the under side. *Lond. Edinb. Dublin Phil. Mag. J. Sci.* **32** (192), 529–546.

ROCHE, P.-E., CASTAING, B., CHABAUD, B. & HÉBRAL, B. 2001 Observation of the 1/2 power law in Rayleigh–Bénard convection. *Phys. Rev.* E **63** (4), 045303.

ROMPS, D. M. 2014 An analytical model for tropical relative humidity. *J. Clim.* **27** (19), 7432–7449.

SCHMIDT, L. E., ORESTA, P., TOSCHI, F., VERZICCO, R., LOHSE, D. & PROSPERETTI, A. 2011 Modification of turbulence in Rayleigh–Bénard convection by phase change. *New J. Phys.* **13** (2), 025002.

SCHUBERT, G. & SODERLUND, K. M. 2011 Planetary magnetic fields: observations and models. *Phys. Earth Plan. Interiors* **187**, 92–108.

SCHUBERT, W. H., HAUSMAN, S. A., GARCIA, M., OOYAMA, K. V. & KUO, H.-C. 2001 Potential vorticity in a moist atmosphere. *J. Atmos. Sci.* **58**, 3148–3157.

SCHUMACHER, J. & PAULUIS, O. 2010 Buoyancy statistics in moist turbulent Rayleigh–Bénard convection. *J. Fluid Mech.* **648**, 509–519.

SCORER, R. S. & LUDLAM, F. H. 1953 Bubble theory of penetrative convection. *Q. J. R. Meteor. Soc.* **79**, 94–103.

SMAGORINSKY, J. 1963 General circulation experiments with the primitive equations. Part I. The basic experiment. *Mon. Wea. Rev.* **91** (3), 99–164.

SMITH, R. K. (Ed.) 2013 *The Physics and Parameterization of Moist Atmospheric Convection*. Springer.

SPIEGEL, E. A. 1971 Convection in stars. Part I. Basic Boussinesq convection. *Annu. Rev. Astron. Astrophys.* **9** (1), 323–352.

SPIEGEL, E. A. & VERONIS, G. 1960 On the Boussinesq approximation for a compressible fluid. *Astrophys. J.* **131**, 442–447. (Correction: *Astrophys. J.*, **135**, 655–656.)

SPYKSMA, K., BARTELLO, P. & YAU, M. K. 2006 A Boussinesq moist turbulence model. *J. Turbul.* **7**, N32.

SUKHATME, J. & YOUNG, W. R. 2011 The advection–condensation model and water-vapour probability density functions. *Q. J. R. Meteor. Soc.* **137**, 1561–1572.

TOMPKINS, A. M. 2001 Organization of tropical convection in low vertical wind shears: the role of cold pools. *J. Atmos. Sci.* **58** (13), 1650–1672.

TSANG, Y.-K. & VANNESTE, J. 2017 The effect of coherent stirring on the advection–condensation of water vapour. *Proc. R. Soc. Lond.* A **473**, 20170196.

VALLIS, G. K. 2017 *Atmospheric and Oceanic Fluid Dynamics*, 2nd edn. Cambridge University Press.

https://doi.org/10.1017/jfm.2018.954 Published online by Cambridge University Press

WEIDAUER, T., PAULUIS, O. & SCHUMACHER, J. 2011 Rayleigh–Bénard convection with phase changes in a Galerkin model. *Phys. Rev.* E **84** (4), 046303.

WHITE, B., GRYSPEERDT, E., STIER, P., MORRISON, H., THOMPSON, G. & KIPLING, Z. 2017 Uncertainty from the choice of microphysics scheme in convection-permitting models significantly exceeds aerosol effects. *Atmos. Chem. Phys.* **17**, 12145–12175.

WHITEHEAD, J. P. & DOERING, C. R. 2011 Ultimate state of two-dimensional Rayleigh–Bénard convection between free-slip fixed-temperature boundaries. *Phys. Rev. Lett.* **106** (24), 244501.

ZHAO, M., GOLAZ, J.-C., HELD, I. M., RAMASWAMY, V., LIN, S.-J., MING, Y., GINOUX, P., WYMAN, B., DONNER, L. J., PAYNTER, D. *et al.* 2016 Uncertainty in model climate sensitivity traced to representations of cumulus precipitation microphysics. *J. Clim.* **29** (2), 543–560.

https://doi.org/10.1017/jfm.2018.954 Published online by Cambridge University Press